Modelling the Photosynthetic Water Oxidation Center. Preparation and Properties of Tetranuclear Manganese Complexes Containing $[Mn_4O_2]^{6+,7+,8+}$ Cores and the Crystal Structures of $Mn_4O_2(O_2CMe)_6(bipy)_2$ and $[Mn_4O_2(O_2CMe)_7(bipy)_2](ClO_4)$

John B. Vincent,[1a] Cheryl Christmas,[1a] Hsiu-Rong Chang,[1c] Qiaoying Li,[1c] Peter D. W. Boyd,[1c,d] John C. Huffman,[1b] David N. Hendrickson,*[1c] and George Christou*[†,1a]

Contribution from the Department of Chemistry and the Molecular Structure Center, Indiana University, Bloomington, Indiana 47405, and the School of Chemical Sciences, University of Illinois, Urbana, Illinois 61801. *Received June 6, 1988*

Abstract: An inorganic model approach to the photosynthetic water oxidation enzyme has been initiated, and synthetic entry into tetranuclear Mn complexes containing $[Mn_4O_2]^{6+,7+,8+}$ cores has been achieved. They have been obtained by bipyridine (bipy)-mediated conversion of trinuclear $[Mn_3O]$-containing species, with the product oxidation level governed by the exact identity of the $[Mn_3O]$ reagent employed. Treatment of $Mn_3O(O_2CMe)_6(py)_3$ with ~3 equiv of bipy in MeCN yields $Mn_4O_2(O_2CMe)_6(bipy)_2$ (**1**) in 91% yield. Complex **1**·$2CHCl_3$ crystallizes in triclinic space group $P\bar{1}$ with (at -160 °C) a = 13.883 (3) Å, b = 10.592 (2) Å, c = 8.848 (1) Å, α = 91.18 (1)°, β = 72.14 (1)°, γ = 71.44 (1)°, V = 1163.84 Å^3, and Z = 1. A total of 3064 unique data with $F > 3\sigma(F)$ were refined to values of R and R_w of 3.23 and 3.75%, respectively. The molecule lies on an inversion center and contains a planar Mn_4 rhombus with two μ_3-O atoms, one above and one below the Mn_4 plane. The resulting $[Mn_4O_2]^{6+}$ core is mixed valence ($2Mn^{II}$, $2Mn^{III}$) and can be considered as fusion of two Mn_3O units by edge-sharing. Peripheral ligation is by six μ_2-O_2CMe and two terminal bipy groups to yield a complex with imposed C_i symmetry. Treatment of $Mn_3O(O_2CR)_6(py)_2(H_2O)$ (R = Ph, 3-Me-Ph) with ~3 equiv of bipy in MeCN yields $Mn_4O_2(O_2CR)_7(bipy)_2$ (R = Ph (**2**) or 3-Me-Ph (**3**)) containing Mn^{II}, $3Mn^{III}$. Similarly, treatment of $[Mn_3O(O_2CR)_6(py)_3](ClO_4)$ (R = Me, Et, Ph) with ~3 equiv of bipy in MeCN yields $[Mn_4O_2(O_2CR)_7(bipy)_2](ClO_4)$ (R = Me (**4**), Et (**8**), Ph (**9**)) containing $4Mn^{III}$. Use of 4,4′-Me_2-bipy instead of bipy results in the corresponding complex $[Mn_4O_2(O_2CMe)_7(4,4'\text{-}Me_2\text{-}bipy)_2](ClO_4)$ (**5**). Complex **4** has been found to undergo facile carboxylate substitution when more acidic carboxylic acids are added; addition of PhCOOH or HCOOH to CH_2Cl_2 solutions of **4** yields **9** and $[Mn_4O_2(O_2CH)_7(bipy)_2](ClO_4)$ (**6**), respectively. Complex **9** can also be synthesized directly by reaction of $NBu^n_4MnO_4$ with $Mn(O_2CMe)_2{\cdot}4H_2O$ in pyridine solution in the presence of PhCOOH, bipy, and $NBu^n_4ClO_4$. Complex **4** crystallizes in triclinic space group $P\bar{1}$ with (at -155 °C) a = 21.133 (11) Å, b = 11.428 (5) Å, c = 11.839 (6) Å, α = 102.12 (2)°, β = 119.72 (2)°, γ = 78.20 (2)°, V = 2410.61 Å^3, and Z = 2. A total of 6294 unique data were refined to values of R and R_w of 9.05 and 8.94%, respectively. Complex **4** contains an $[Mn_4O_2]^{8+}$ core which is not planar as found in **1** but exhibits an Mn_4 butterfly arrangement with both μ_3-O atoms on the same side of the molecule. Peripheral ligation is again by μ_2-O_2CMe and terminal bipy groups, but now there is an additional $MeCO_2^-$ ligand bridging the two "hinge" Mn atoms of the butterfly to yield C_2 symmetry. Complexes **1** and **4** display both "short" and "long" Mn···Mn separations, 2.779 (1), 3.288-3.481 (1) Å and 2.848 (5), 3.312-3.385 (5) Å, respectively. Variable-temperature, solid-state, magnetic-susceptibility studies have been performed on representative complexes **1** and **4** in the temperature range 5-300 K. The observed susceptibility data have been fitted to models involving isotropic exchange interactions between the high-spin manganese ions in the clusters. In the case of $Mn^{II}_2Mn^{III}_2$ complex **1**, fitting the data gave $J_{13} = -3.12$ cm^{-1} for the interaction between the two di-μ-oxo-bridged Mn^{III} ions and $J(Mn^{II}\text{–}Mn^{III}) = -1.97$ cm^{-1}. With these parameters, complex **1** has an S = 2 ground state with six other spin states within 15 cm^{-1}. Fitting the data for Mn^{III}_4 complex **4** gave for the di-μ-oxo-bridged Mn^{III} pair $J_{13} = -23.5$ cm^{-1}, and for the other $Mn^{III}\text{–}Mn^{III}$ interaction $J = -7.8$ cm^{-1}. The ground state for **4** has S = 3 with two lowest lying excited states being two energetically degenerate S = 2 states at ~15 cm^{-1} above the S = 3 ground state. The nature of the ground and low-lying spin states for **1** and **4** were confirmed by using magnetization measurements at fields up to 48 kG and temperatures down to 1.8 K. The change in the magnitude of spin–spin interaction between the two central di-μ-oxo-bridged Mn^{III} ions in **1** and **4** can be related to the differing single-ion coordination in these two complexes. The electronic difference spectrum of the $[Mn_4O_2(O_2CPh)_7(bipy)_2]^{0,+}$ pair has been found to be extremely similar to the $S_0 \rightarrow S_1$ difference spectrum of the water oxidation site, suggesting the latter involves a $Mn^{II} \rightarrow Mn^{III}$ transition also. Complex **4** in $CDCl_3$ has been found to display a well-resolved ^1H NMR spectrum in which all expected proton resonances have been located and assigned. Both σ and π spin-delocalization mechanisms appear to be operative. The combined results of this work are discussed with respect to their biological relevance, and it is proposed that complexes containing the $[Mn_4O_2]^{6+,7+,8+}$ cores represent potential synthetic analogues of the S_{-1}, S_0, and S_1 states, respectively, of the water oxidation enzyme.

Intense effort is currently being concentrated on elucidating the nature of the biological unit responsible for water oxidation/oxygen evolution in the photosynthetic apparatus of green plants and cyanobacteria. It is believed that the site for water oxidation is a tetranuclear Mn aggregate operating on the donor side of Photosystem II (PS II).[2] The four Mn atoms are essential for activity and appear to be in close proximity to one another.[3-5] The Mn atoms are apparently heterogeneous, being composed of two pools of two similar atoms.[6,7] The complete Mn_4 aggregate is capable of cycling between five distinct oxidation levels labeled S_0–S_4 in the pioneering work of Kok[8] but can also adopt a "super-reduced" S_{-1} state under certain conditions.[9,10] The S_n

[†] Alfred P. Sloan Research Fellow, 1987-1989; Camille and Henry Dreyfus Teacher-Scholar, 1987-1992.

(1) (a) Indiana University Chemistry Department. (b) Indiana University Molecular Structure Center. (c) University of Illinois. (d) On sabbatical leave from the University of Auckland, Auckland, New Zealand.

(2) Amesz, J. *Biochim. Biophys. Acta* **1983**, *726*, 1. Dismukes, G. C. *Photochem. Photobiol.* **1986**, *43*, 99.

(3) Dismukes, G. C.; Ferris, K.; Watnick, P. *Photochem. Photobiol.* **1982**, *3*, 243.

(4) Kirby, J. A.; Robertson, A. S.; Smith, J. P.; Thompson, A. C.; Cooper, S. R.; Klein, M. P. *J. Am. Chem. Soc.* **1981**, *103*, 5529.

(5) Kulikov, A. F.; Bogatyrenko, V. R.; Likhtenshtein, G. J.; Allakhverdiyev, S. J.; Klimov, V. V.; Shulalov, V. A.; Krasnovskii, A. A. *Biophysics* **1983**, *28*, 381.

0002-7863/89/1511-2086$01.50/0

states contain Mn in various combinations of the higher metal oxidation states (II–IV), and ligation is provided by O,N-based groups from amino acid side-chain functions viz histidine, tyrosine, and aspartic/glutamic acids; no porphyrins have been detected, and all quinones have been accounted for in other functions.[11]

Despite much effort to date, hardly any synthetic Mn_4 complexes have hitherto been available to function as models of the biological site.[12] Such low molecular weight materials would be invaluable to assist in continuing attempts to elucidate structural and mechanistic aspects of the water oxidation cycle and to aid in the interpretation of data from EPR, EXAFS and other physical techniques currently employed. We now report the successful synthesis of tetranuclear Mn complexes which possess sufficient structural and other features similar to the native site to suggest that synthetic models may have been obtained should it prove to be tetranuclear. Preliminary results have been reported briefly elsewhere.[13-15]

Experimental Section

Syntheses. All manipulations were performed under aerobic conditions with use of materials as received. Trinuclear $[Mn_3O]$ complexes were available from previous work[16] except complex **7** whose preparation is reported below for the first time. $NBu^n_4MnO_4$ was prepared as described.[17] **WARNING**: Appropriate care should be taken in the use of $NBu^n_4MnO_4$, and readers are referred to the detailed warning given elsewhere.[17]

$[Mn_4O_2(O_2CMe)_6(bipy)_2]\cdot 2CHCl_3$ (1). A stirred brown solution of $[Mn_3O(O_2CMe)_6(py)_3](py)$ (0.85 g, 1.0 mmol) in MeCN (30 mL) was treated with solid bipy (0.50 g, 3.2 mmol). From the resulting homogeneous red solution, a fine reddish powder of **1** precipitated in ca. 91% yield. The solid was collected by filtration, washed with MeCN, and dried in vacuo. Recrystallization from $CHCl_3$/MeCN or $CHCl_3$/hexanes yields well-formed, dark red crystals of the bis-$CHCl_3$ solvate. Anal. Calcd for $C_{34}H_{36}N_4O_{14}Cl_6Mn_4$: C, 35.3; H, 3.1; N, 4.8; Mn, 19.0. Found: C, 35.7; H, 3.2; N, 4.7; Mn, 19.2. Electronic spectrum in CH_2Cl_2, λ_{max}, nm (ϵ_M/Mn_4, $L\cdot mol^{-1}\ cm^{-1}$) 466 (820), 508 (772). IR data 1595 (s), 1560 (s), 1340 (m), 1315 (w), 1275 (w), 1245 (w), 1215 (w), 1170 (w), 1150 (m), 1065 (m), 1015 (s), 930 (w), 895 (w), 765 (s), 745 (s), 735 (s), 645 (s), 620 (m), 605 (w).

$Mn_4O_2(O_2CPh)_7(bipy)_2$ (2). To a stirred green-brown solution of $[Mn_3O(O_2CPh)_6(py)_2(H_2O)]\cdot{}^1/_2MeCN$ (1.10 g, 1.0 mmol) in MeCN (25 mL) was added solid bipy (0.50 g, 3.2 mmol). The resulting brown solution began to precipitate brown microcrystals of **2** within minutes. After 1 h, the solid was collected by filtration, washed with MeCN, and dried; yield 60–70%. Recrystallization can be effected from CH_2Cl_2/MeCN or CH_2Cl_2/hexanes to give large black prisms which have repeatedly proven to be poor diffractors of X-rays. Anal. Calcd for $C_{69}H_{51}N_4O_{16}Mn_4$: C, 58.70; H, 3.64; N, 3.97; Mn, 15.6. Found: C, 58.39; H, 3.84; N, 3.92; Mn, 15.4. Electronic spectrum in DMF 428 (1326), 472 (1116). IR data 1605 (s), 1570 (s), 1315 (w), 1275 (w), 1250 (w), 1175 (m), 1160 (m), 1140 (w), 1090 (m), 1065 (m), 1025 (m), 835 (m), 765 (m), 720 (s), 670 (s), 645 (s), 465 (m).

$Mn_4O_2(O_2CPh\text{-}3\text{-}Me)_7(bipy)_2$ (3). The complex $Mn_3O(O_2CPh\text{-}3\text{-}Me)_6(py)_2(H_2O)$ was obtained in 97% yield by a procedure analogous to that for the $PhCO_2^-$ complex.[16] To a stirred green-brown solution of $Mn_3O(O_2CPh\text{-}3\text{-}Me)_6(py)_2(H_2O)$ (0.58 g, 0.5 mmol) in MeCN (15 mL) was added solid bipy (0.25 g, 1.6 mmol). The resulting red-brown solution was filtered to remove a small amount of a gold-colored precipitate, and the filtrate was concentrated in vacuo to an oil. This was dissolved in CH_2Cl_2 (~20 mL) and filtered, and the filtrate was layered with an equal volume of MeCN. After several days, the well-formed dark red crystals were collected by filtration, washed with MeCN, and dried in vacuo; yield 49%. Anal. Calcd for $Mn_4N_4O_{16}C_{76}H_{65}$: C, 60.5; H, 4.3; N, 3.7; Mn, 14.6. Found: C, 60.8; H, 4.3; N, 3.9; Mn, 14.2. Electronic spectrum in CH_2Cl_2 462 (1281), 506 (1089). IR data 1615 (s), 1600 (s), 1580 (s), 1545 (s), 1280 (s), 1275 (s), 1210 (s), 1155 (m), 1080 (m), 1055 (m), 1030 (m), 1015 (m), 900 (w), 780 (s), 755 (s), 730 (s), 670 (s), 635 (s), 520 (m), 490 (m), 455 (m).

$[Mn_4O_2(O_2CMe)_7(bipy)_2](ClO_4)\cdot 3H_2O$ (4). To a stirred brown solution of $[Mn_3O(O_2CMe)_6(py)_3](ClO_4)$ (0.87 g, 1.0 mmol) in MeCN (30 mL) was added solid bipy (0.50 g, 3.2 mmol). The resulting deep red solution was layered with a 1:1 mixture of hexanes and Et_2O (30 mL). Slow mixing yielded dark red crystals of **4** as the tris-H_2O solvate. The crystals were collected by filtration, washed with Et_2O, and dried; yield ca. 70%. Recrystallization from CH_2Cl_2/Et_2O gives large dark red crystals. Anal. Calcd for $C_{34}H_{43}N_4O_{23}ClMn_4$: C, 36.11, H, 3.83; N, 4.95; Mn, 19.43. Found: C, 36.29; H, 3.76; N, 4.59; Mn, 18.62. Electronic spectrum in CH_2Cl_2 412 (1064), 447 (1072), 504 (1004). IR data: 3500 (s, br), 1590 (s), 1320 (w), 1280 (w), 1245 (w), 1175 (m), 1160 (m), 1090 (s), 1030 (m), 1020 (w), 1280 (w), 1245 (w), 1175 (m), 1160 (m), 1090 (s), 1030 (m), 1020 (w), 930 (w), 770 (s), 730 (s), 660 (s), 645 (m), 615 (s), 600 (sh).

$[Mn_4O_2(O_2CCD_3)_7(bipy)_2](ClO_4)$ was obtained by an identical procedure employing $[Mn_3O(O_2CCD_3)_6(py)_3](ClO_4)$.

$[Mn_4O_2(O_2CMe)_7(4,4'\text{-}Me_2\text{-}bipy)_2](ClO_4)\cdot H_2O$ (5). To a stirred solution of $[Mn_3O(O_2CMe)_6(py)_3](ClO_4)$ (0.44 g, 0.50 mmol) in CH_2Cl_2 (10 mL) was added solid 4,4'-dimethylbipyridine (0.28 g, 1.50 mmol). As the solid dissolved, the initially brown solution turned red. After ~30 min, Et_2O was added dropwise until precipitation of red microcrystals of complex **5** was complete. These were collected by filtration, washed with Et_2O, and dried in vacuo; yield 46%. Anal. Calcd for $C_{38}H_{47}N_4O_{21}ClMn_4$: C, 39.7; H, 4.4; N, 4.87. Found: C, 39.8; H, 3.9; N, 5.25. Electronic spectrum in CH_2Cl_2 404 (1080), 446 (1055), 502 (980). IR data 3450 (m, br), 1610 (s), 1590 (s), 1555 (m), 1340 (m), 1285 (m), 1245 (m), 1095 (s), 1030 (m), 935 (m), 830 (m), 725 (m), 675 (m), 660 (sh), 650 (s), 620 (m), 600 (m), 570 (w), 520 (m).

$[Mn_4O_2(O_2CH)_7(bipy)_2](ClO_4)\cdot{}^3/_4CH_2Cl_2$ (6). To a stirred solution of complex **4** (0.57 g, 0.50 mmol) in CH_2Cl_2 (20 mL) was added formic acid (0.50 mL, 8.9 mmol). No noticeable color change occurred, but, after a few minutes, a red microcrystalline precipitate of **6** was deposited. After ~30 min, the solid was collected by filtration, washed with Et_2O, and dried in vacuo; yield 88%. Anal. Calcd for $C_{27.75}H_{24.5}N_4O_{20}Cl_{2.5}Mn_4$: C, 32.0; H, 2.4; N, 5.4; Mn, 21.1. Found: C, 32.4; H, 2.5; N, 5.3; Mn, 21.1. Electronic spectrum in DMF 503 (sh, 875). IR data 1600 (s), 1550 (s), 1330 (m), 1280 (w), 1250 (m), 1160 (m), 1145 (w), 1090 (s), 1030 (m), 900 (w), 775 (s), 750 (m), 725 (s), 665 (s), 655 (s), 635 (s), 620 (s), 590 (m), 455 (m), 420 (m).

$[Mn_3O(O_2CEt)_6(py)_3](ClO_4)$ (7). To a stirred solution of $Mn(O_2CMe)_2\cdot 4H_2O$ (2.00 g, 8.15 mmol) in a mixture of EtOH (20 mL), propionic acid (12 mL), and pyridine (3 mL) was slowly added $NBu^n_4MnO_4$ (1.14 g, 3.15 mmol) in small portions. $NaClO_4$ (0.69 g, 5.6 mmol) was dissolved in the resulting brown solution, and the flask was stored at −10 °C overnight to give black crystals of complex **7**. These were collected by filtration, washed with Et_2O, and dried in vacuo; yield 60%. Anal. Calcd for $C_{33}H_{45}N_3O_{17}ClMn_3$: C, 41.5; H, 4.7; N, 4.4; Mn, 17.2. Found: C, 41.1; H, 4.6; N, 4.4; Mn, 17.1. IR data 1600 (vs), 1390 (s), 1220 (s), 1160 (m), 1085 (vs), 1045 (m), 1020 (m), 885 (m), 815 (m), 760 (m), 685 (s), 645 (s), 620 (s), 590 (m), 445 (m).

$[Mn_4O_2(O_2CEt)_7(bipy)_2](ClO_4)$ (8). To a stirred brown solution of complex **7** (1.80 g, 1.9 mmol) in acetone (20 mL) was added solid bipy (0.95 g, 6.1 mmol) to give a red solution. Et_2O (~20 mL) was added, and the flask was stored at −10 °C overnight to give red microcrystals of **8**. These were collected by filtration, washed with Et_2O, and dried in vacuo; yield 90%. Anal. Calcd for $C_{41}H_{51}N_4O_{20}ClMn_4$: C, 41.9; H, 4.4; N, 4.8; Mn, 18.7. Found: C, 41.9; H, 4.3; N, 4.7; Mn, 18.3. Electronic spectrum in CH_2Cl_2 415 (1004), 448 (920), 501 (860). IR data 1605 (s), 1580 (s), 1560 (s), 1320 (m), 1290 (m), 1280 (m), 1250 (m), 1175 (m), 1160 (m), 1125 (m), 1105 (s), 1085 (s), 1030 (m), 880 (m), 810 (m), 775 (s), 750 (m), 730 (s), 660 (s), 650 (s), 640 (m), 620 (s), 600 (s), 415 (m).

$[Mn_4O_2(O_2CPh)_7(bipy)_2](ClO_4)$ (9). Method A. To a stirred brown solution of $[Mn_3O(O_2CPh)_6(py)_3](ClO_4)\cdot 0.5CH_2Cl_2$ (1.29 g, 1.0 mmol) in CH_2Cl_2 (30 mL) was added solid bipy (0.50 g, 3.2 mmol) to give a red solution. Careful layering with Et_2O (30 mL) gave, after several days, large dark red needles of **9**. These were collected by filtration, washed with Et_2O, and dried in vacuo; yield 80%. Anal. Calcd for $C_{69}H_{51}N_4O_{20}ClMn_4$: C, 54.8; H, 3.4; N, 3.7; Mn, 14.5. Found: C, 54.4; H, 3.4; N, 3.7; Mn, 14.5. Electronic spectrum in CH_2Cl_2 466 (1120),

(6) Kuwabara, T.; Miyao, M.; Murata, N. *Biochim. Biophys. Acta* **1985**, *806*, 283.
(7) Klimov, V. V.; Allakhverdiev, S. J.; Shulalov, V. A.; Krasnovsky, A. A. *FEBS Lett.* **1982**, *148*, 307.
(8) Kok, B.; Forbush, B.; McGloin, M. *Photochem. Photobiol.* **1970**, *11*, 457.
(9) Velthuys, B.; Kok, B. *Biochim. Biophys. Acta* **1978**, *502*, 211.
(10) Pistorius, E. K.; Schmid, G. H. *Biochim. Biophys. Acta* **1987**, *898*, 352.
(11) Takohashi, Y.; Katoh, S. *Biochim. Biophys. Acta* **1986**, *848*, 183.
(12) Wieghardt, K.; Bossek, U.; Gebert, W. *Angew. Chem., Int. Ed. Engl.* **1983**, *22*, 328.
(13) Vincent, J. B.; Christmas, C.; Huffman, J. C.; Christou, G.; Chang, H.-R.; Hendrickson, D. N. *J. Chem. Soc., Chem. Commun.* **1987**, 236.
(14) Vincent, J. B.; Christou, G. *FEBS Lett.* **1986**, *207*, 250.
(15) Christmas, C.; Vincent, J. B.; Huffman, J. C.; Christou, G.; Chang, H.-R.; Hendrickson, D. N. *J. Chem. Soc., Chem. Commun.* **1987**, 1303.
(16) Vincent, J. B.; Chang, H.-R.; Folting, K.; Huffman, J. C.; Christou, G.; Hendrickson, D. N. *J. Am. Chem. Soc.* **1987**, *109*, 5703.
(17) Vincent, J. B.; Folting, K.; Huffman, J. C.; Christou, G. *Inorg. Chem.* **1986**, *25*, 996.

Table I. Crystallographic Data for Complexes 1 and 4

parameter	1	4
formula	$C_{34}H_{36}N_4O_{14}Cl_6Mn_4$	$C_{34}H_{43}N_4O_{23}ClMn_4$
M_r	1157.72	1130.96
cryst system	triclinic	triclinic
space group	$P\bar{1}$	$P\bar{1}$
temp, °C	−160	−155
a, Å	13.883 (3)[a]	21.133 (11)[b]
b, Å	10.592 (2)	11.428 (5)
c, Å	8.848 (1)	11.839 (6)
α, deg	91.18 (1)	102.12 (2)
β, deg	72.14 (1)	119.72 (2)
γ, deg	71.44 (1)	78.20 (2)
V, Å^3	1163.84	2410.61
Z	1	2
cryst dimens, mm	0.24 × 0.24 × 0.30	0.18 × 0.18 × 0.34
radiation,[c] Mo Kα, Å	0.71069	0.71069
abs, coeff, cm^{-1}	14.283	11.101
scan speed, deg/min	4.0	4.0
scan width, deg	2.0 + dispersion	2.0 + dispersion
data collcd	$6° \le 2\theta \le 45°$	$6° \le 2\theta \le 45°$
total data	3689	6895
unique data	3064	6294
averaging R[d]	0.043	0.094
obsd data	2867, $F > 3\sigma(F)$	2434, $F > 2.33\sigma(F)$
R,[e] %	3.23	9.05
R_w,[f] %	3.75	8.94
goodness of fit[g]	1.287	1.564

[a] 32 reflections. [b] 40 reflections. [c] Graphite monochromator. [d] 625 and 601 reflections, respectively, measured more than once. [e] $R = \sum||F_o| - |F_c||/\sum F_o|$. [f] $R_w = [\sum w(|F_o| - |F_c|)^2/\sum w|F_o|^2]^{1/2}$ where $w = 1/\sigma^2(|F_o|)$. [g] Goodness of fit = $[\sum w(|F_o| - |F_c|)^2/(N_{obsns} - N_{paras})]^{1/2}$.

508 (1092). IR data 1605 (s), 1570 (s), 1305 (w), 1280 (w), 1250 (w), 1175 (m), 1160 (m), 1140 (w), 1095 (s), 1070 (m), 1035 (m), 1000 (m), 935 (w), 835 (m), 815 (w), 770 (s), 720 (s), 665 (m), 620 (m), 600 (m), 470 (m).

Method B. Benzoic acid (1.22 g, 10 mmol) was dissolved in a solution of complex **4** (0.57 g, 0.5 mmol) in CH_2Cl_2 (30 mL). The solution was then carefully layered with Et_2O (30 mL), and, after several days, the resulting dark red crystals were isolated as above in comparable yield.

Method C. To a stirred solution of $Mn(O_2CMe)_2{\cdot}4H_2O$ (2.00 g, 8.15 mmol) and benzoic acid (7.50 g, 61 mmol) in pyridine (20 mL) was added solid $NBu^n_4MnO_4$ (1.95 g, 5.40 mmol) in small portions to give a red-brown solution. After a further few minutes, bipy (2.55 g, 16.3 mmol) and $NBu^n_4ClO_4$ (3.00 g, 8.77 mmol) were added, and the resulting solution was stripped to dryness in vacuo. The residue was extracted with separate portions of EtOH (50–75 mL) and MeCN (~50 mL), and each extract was filtered and allowed to concentrate by evaporation to yield red crystals of **9**. Both crops were identical on spectroscopic examination, and the combined yield was ~60%.

X-ray Crystallography. Data were collected on a Picker four-circle diffractometer at −160 and −155 °C for **1** and **4**, respectively; details of the diffractometry, low-temperature facilities, and computational procedures employed by the Molecular Structure Center are available elsewhere.[18] Data collection parameters are summarized in Table I. For both complexes, a systematic search of a limited hemisphere of reciprocal space located a set of diffraction maxima with no symmetry or systematic absences indicating a triclinic space group. Subsequent solution and refinement of the structures confirmed the centrosymmetric choice $P\bar{1}$. The structures were solved by a combination of direct methods (MULTAN) and Fourier techniques and refined by full-matrix least squares.

For complex **1**, all non-hydrogen atoms were readily located, including those of a well-behaved $CHCl_3$ solvent molecule. These were refined with anisotropic thermal parameters. In the latter stages, the positions of all hydrogen atoms were clearly visible in a difference Fourier phased on the non-hydrogen atoms, and the coordinates and isotropic thermal parameters were varied in the final refinement cycles. A final difference Fourier was essentially featureless with the largest peak being 0.53 e/Å^3.

For complex **4**, all non-hydrogen atoms were readily located except for those of seriously disordered water molecules. Except for the latter which were refined isotropically, all non-hydrogen atoms were refined with anisotropic thermal parameters. No hydrogen atoms were visible in a difference Fourier phased on the non-hydrogen atoms, so no attempt was made to include them in the final refinement cycles. A final difference Fourier was essentially featureless with the largest peak being 0.40 e/Å^3.

Other Measurements. Variable-temperature magnetic susceptibility data were measured with a series 800 VTS-50 SQUID susceptometer (S.H.E. Corp.) maintained by the University of Illinois Physics Department. The susceptometer was operated at a magnetic field strength of 10 kG. Diamagnetic corrections were estimated from Pascal's constants and subtracted from the experimental susceptibility data to obtain the molar paramagnetic susceptibilities of the compounds. These molar paramagnetic susceptibilities were fit to the appropriate theoretical expressions by means of a least-squares-fitting computer program.[19] Bulk magnetization measurements were performed on vaseline mulls of the complexes to prevent orientation effects at higher fields and lower temperatures due to magnetic anisotropies of the crystallites.

Infrared (Nujol mull) and electronic solution spectra were recorded on Perkin-Elmer Model 283 and Hewlett-Packard Model 4450A spectrophotometers, respectively. ^1H NMR spectra were recorded in $CDCl_3$ solution at ~23 °C with a Nicolet NT-360 spectrometer. Chemical shifts are quoted on the δ scale (shifts downfield are positive) with the $CDCl_3$ protio-signal as a reference (δ = 7.26). Elemental analyses were performed at the Microanalytical Laboratory, Department of Chemistry, Manchester University, England.

Results and Discussion

Syntheses. Previous work had established that $NBu^n_4MnO_4$ in nonaqueous solvents represents a useful new synthetic route into higher oxidation state Mn chemistry.[16,17] In particular, a variety of trinuclear $[Mn_3O(O_2CR)_6L_3]^{0,+}$ (R = Me, Et, Ph; L = pyridine (py), imidazole (HIm), H_2O) complexes had been obtained in high yield by a straightforward, one-pot reaction.[16] With these complexes at hand in large amounts, we wondered whether a means could be developed for their conversion to tetranuclear species more potentially relevant to the water oxidation site near PS II. Alternatively, we wondered whether appropriate modification to the $NBu^n_4MnO_4$ reaction system might instead yield tetranuclear species directly. The current status of our work has established that both of the above objectives can be fulfilled, but initial success came from the former approach, and this represents the routine procedure we have continued to employ and shall describe in more detail.

Two potential ways of converting Mn_3O to Mn_4 species were investigated. One method was to react Mn_3O complexes with bulky carboxylates hoping that six of the latter could not be accommodated, and thus lead to higher nuclearity products containing a lower $RCOO^-/Mn$ ratio. We employed ligands such as 2,6-dimethoxybenzoic acid and 2-phenylbenzoic acid, but in all cases found messy reactions and/or mixtures of products difficult to separate. This approach was thus abandoned. The second method was to react Mn_3O complexes with chelating ligands since these could not be readily incorporated around the Mn_3O core without serious disruption, which might again lead to aggregation (although formation of lower nuclearity products seemed equally possible). The ligand chosen was 2,2′-bipyridine (bipy), and this proved to be highly successful and yielded exactly the nuclearity desired, namely four.

The Experimental Section lists nine Mn_4O_2 complexes in order of increasing oxidation level; the first complex obtained was actually **4**. Treatment of $[Mn_3O(O_2CMe)_6(py)_3](ClO_4)$ with just over 3 equiv of bipy in MeCN led to a rapid color change from brown to dark red. Layering of the solution with a mixture of Et_2O and hexanes (1:1) gave highly crystalline **4** in ~70% yield. The complex is air-stable and soluble in solvents such as CH_2Cl_2 without change. A structural characterization established the formulation $[Mn_4O_2(O_2CMe)_7(bipy)_2](ClO_4){\cdot}3H_2O$; its preparation is summarized in eq 1. The increase in the O/Mn ratio

$$\tfrac{4}{3}[Mn_3O(O_2CMe)_6(py)_3](ClO_4) + 4bipy + \tfrac{2}{3}H_2O \rightarrow [Mn_4O_2(O_2CMe)_7(bipy)_2](ClO_4) + 2bipy + MeCOOH + \tfrac{1}{3}HClO_4 + 3py \quad (1)$$

in the product suggests involvement of H_2O from the solvent, and

(18) Chisholm, M. H.; Folting, K.; Huffman, J. C.; Kirkpatrick, C. C. *Inorg. Chem.* **1984**, *23*, 1021.

(19) Chandler, J. P. Program 66; Quantum Chemistry Program Exchange, Indiana University, Bloomington, IN.

eq 1 is balanced accordingly. The Mn_3O parenthood of the Mn_4O_2 product is reflected in its structure; the latter can be described as two Mn_3O triangles fused together by sharing an edge (vide infra). Note that in this reaction there is no change in metal oxidation state (+3.0).

The procedure in eq 1 has been extended by appropriate change in the precise identities of the carboxylate and bipy to yield the corresponding complexes, viz **5**, **8**, **9**, and the O_2CCD_3 version of **4**. No doubt this synthetic approach could also be extended to still more carboxylates and other amines such as 1,10-phenanthroline.

A more significant change in the identity of the product came about when Mn_3O complexes in a lower average metal oxidation state (+2.67) were employed. Treatment of $Mn_3O(O_2CPh)_6(py)_2(H_2O)$ with ~3 equiv of bipy yielded a brown microcrystalline precipitate. Recrystallization from CH_2Cl_2/MeCN or CH_2Cl_2/hexanes yields large, well-formed black prisms which, unfortunately, have repeatedly proven to be poor diffractors of X-rays. Its IR and complete elemental analysis indicate this product to be neutral $Mn_4O_2(O_2CPh)_7(bipy)_2$ (**2**), soluble in CH_2Cl_2 and THF. Its formation is summarized in eq 2. The

$$\tfrac{4}{3}Mn_3O(O_2CPh)_6(py)_2(H_2O) + 4bipy \rightarrow Mn_4O_2(O_2CPh)_7(bipy)_2 + PhCOOH + \tfrac{2}{3}H_2O + \tfrac{8}{3}py + 2bipy \quad (2)$$

average metal oxidation state of the product (+2.75) is greater than the Mn_3O reagent (+2.67), suggesting either involvement of atmospheric O_2 or some lower oxidation state (Mn^{II}) byproduct. We have been unable to isolate any other Mn product from the reaction filtrate for identification but, nevertheless, favor the latter possibility, although we refrain from attempting to balance eq 2. The corresponding 3-Me-benzoate derivative **3** can be made in a completely analogous manner but has also proven to possess poor diffraction quality. Overall, a lower oxidation state Mn_3O reagent leads to a lower oxidation state Mn_4O_2 product; however, when the corresponding acetate derivative was sought, hopefully to yield better diffraction properties, this at-first-glance trivial modification to the reaction led to a completely different product.

Treatment of $Mn_3O(O_2CMe)_6(py)_3$ with ~3 equiv of bipy led to precipitation of complex **1** in 91% yield. Analysis and structural characterization established **1** to be $Mn_4O_2(O_2CMe)_6(bipy)_2 \cdot 2CHCl_3$ with a lowered carboxylate/Mn ratio and an average Mn oxidation state of +2.50. Its preparation is summarized in unbalanced eq 3. The identity of the carboxylate used is thus of

$$\tfrac{4}{3}Mn_3O(O_2CMe)_6(py)_3 + 4bipy \rightarrow Mn_4O_2(O_2CMe)_6(bipy)_2 + 2MeCOOH + \tfrac{2}{3}H_2O + 2bipy + 4py \quad (3)$$

paramount importance in governing the obtained product, emphasizing the complexity of these structural and redox rearrangements. Note this time that the average Mn oxidation level in **1** (+2.50) is *lower* than in the starting material (+2.67), suggesting a higher oxidation state byproduct or ligand/solvent oxidation.

Ligand Substitution Reactions. The substitutional lability of representative complex **4** has been investigated. Treatment of a CH_2Cl_2 solution of **4** with 20 equiv of benzoic acid gave a clean and high yield conversion to **9** establishing the lability to substitution of the bound acetate groups, as also observed[20] in $[Mn_2O(O_2CMe)_2(HB(pz)_3)_2]$ ($HB(pz)_3$ = hydrido tris(1-pyrazolyl)borate). Similarly, treatment of **4** with excess formic acid yielded a clean conversion to $[Mn_4O_2(O_2CH)_7(bipy)_2](ClO_4)\cdot{}^3/_4CH_2Cl_2$ (**6**), isolated in 88% yield. These reactions are summarized in eq 4. The reverse reactions, i.e., addition of acetic

$$[Mn_4O_2(O_2CMe)_7(bipy)_2]^+ + 7RCOOH \rightarrow [Mn_4O_2(O_2CR)_7(bipy)_2]^+ + 7MeCOOH \quad (4)$$

acid to **6** or **9** lead to recovery of starting material. This is consistent with the known acidity of the RCOOH molecule as reflected in the pK_a values (4.75 (Me), 4.19 (Ph), and 3.75 (H)) suggesting the probable mechanism to involve protonation of bound acetate by more acidic RCOOH, followed by its displacement by generated $RCOO^-$. Such ligand substitution reactions could have important future consequences, both for incorporating around Mn_4O_2 cores such biologically relevant carboxylates as amino acids or polypeptides or possibly for extruding native Mn clusters from biological units by appropriate carboxylate-containing reagents, akin to core extrusion by acidic thiols of $[Fe_nS_n]$ clusters from non-heme Fe/S proteins and enzymes.[21]

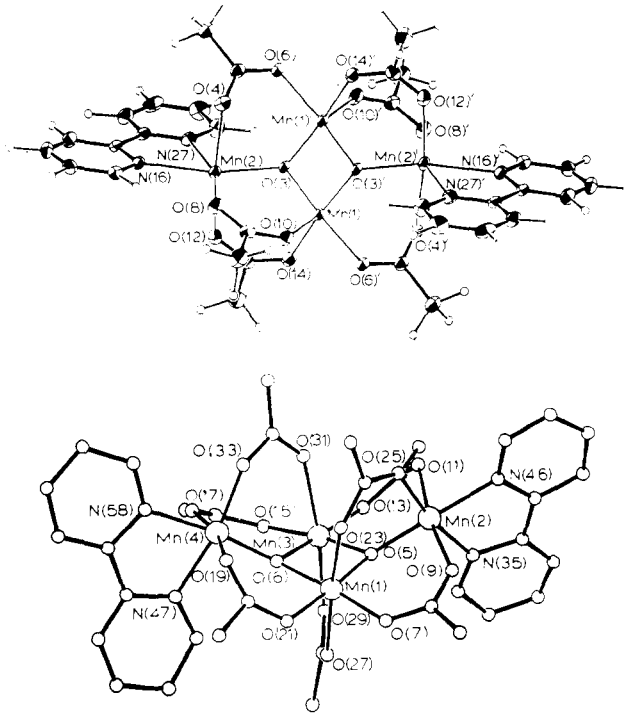

Figure 1. Structure of complex **1** (top) and the cation of complex **4** (bottom) showing the atom labeling scheme. Carbon atoms are labeled consecutively from N and O atoms. Primed and unprimed atoms are related by the inversion center.

As a possible extension to the utility of $NBu^n_4MnO_4$ for inorganic syntheses in nonaqueous solvents, we have investigated whether this reagent could lead directly to Mn_4O_2 complexes, now that a precise ligand combination required to stabilize the latter had been determined. As a representative example, we have sought the preparation of a benzoate species. A solution of $Mn(O_2CMe)_2\cdot 4H_2O$ and benzoic acid in pyridine was treated with $NBu^n_4MnO_4$ followed by addition of $NaClO_4$ and bipy. After workup, complex **9** was isolated in reasonable (~60%) yield. Another successful synthetic use of $NBu^n_4MnO_4$ has thus been established.[22]

Description of Structures. ORTEP projections of complexes **1** and **4** are shown in Figure 1; selected structural parameters are listed in Tables II and III, respectively.

Complex **1** crystallizes in triclinic space group $P\bar{1}$. The asymmetric unit contains half the molecule and one $CHCl_3$ solvate group; the latter will not be further discussed. The complex possesses an exactly planar Mn_4 unit bridged by two μ_3-oxide atoms O(3) and O(3)', one above and one below the Mn_4 plane.

(20) Sheats, J. E.; Czernuszewicz, R. S.; Dismukes, G. C.; Rheingold, A. L.; Petrouleas, V.; Stubbe, J.; Armstrong, W. H.; Beer, R. H.; Lippard, S. J. *J. Am. Chem. Soc.* **1987**, *109*, 1435.

(21) (a) Holm, R. H. In *Biological Aspects of Inorganic Chemistry*; Addison, A. W., Cullen, W. R., Dolphin, D., James, B. R., Eds.; Wiley-Interscience: New York, 1977; pp 71-111. (b) Coles, C. J.; Holm, R. H.; Kurtz, D. M.; Orme-Johnson, W. H.; Rawlings, J.; Singer, T. P.; Wong, G. B. *Proc. Natl. Acad. Sci. U.S.A.* **1979**, *76*, 3805. (c) Kurtz, D. M.; McMilland, R. S.; Burgess, B. K.; Mortenson, L. E.; Holm, R. H. *Proc. Natl. Acad. Sci. U.S.A.* **1979**, *76*, 4986.

(22) The direct synthesis of $Mn_4O_2(O_2CCPh_3)_6(Et_2O)_2$ has recently been communicated: Kulawiec, R. J.; Crabtree, R. H.; Brudvig, G. W.; Schulte, G. K. *Inorg. Chem.* **1988**, *27*, 1309.

Table II. Selected Bond Distances (Å) and Angles (deg) for **1**

a. Bonds

Mn(1)···Mn(1)′	2.779 (1)	Mn(1)-O(3)	1.8507 (20)
Mn(1)···Mn(2)	3.288 (1)	Mn(1)-O(3)′	1.8560 (21)
Mn(1)···Mn(2)′	3.481 (1)	Mn(2)-O(3)	2.1032 (21)
Mn(1)-O(6)	1.9798 (21)	Mn(2)-O(8)	2.1208 (22)
Mn(1)-O(10)	2.1180 (22)	Mn(2)-O(12)	2.1912 (23)
Mn(1)-O(14)	1.9770 (21)	Mn(2)-N(16)	2.2597 (26)
Mn(2)-O(4)	2.2278 (22)	Mn(2)-N(27)	2.2671 (27)

b. Angles

Mn(1)-O(3)-Mn(1)′	97.12 (10)	O(3)-Mn(2)-O(8)	106.18 (8)
Mn(1)-O(3)-Mn(2)	112.36 (10)	O(3)-Mn(2)-O(12)	85.75 (8)
Mn(1)′-O(3)-Mn(2)	122.99 (10)	O(3)-Mn(2)-N(16)	163.50 (9)
O(3)-Mn(1)-O(6)′	169.91 (9)	O(3)-Mn(2)-N(27)	92.46 (9)
O(3)-Mn(1)-O(3)′	82.88 (10)	O(4)-Mn(2)-O(8)	94.13 (9)
O(3)-Mn(1)-O(10)	104.31 (9)	O(4)-Mn(2)-O(12)	170.88 (8)
O(3)-Mn(1)-O(14)	93.38 (9)	O(4)-Mn(2)-N(16)	87.22 (9)
O(3)′-Mn(1)-O(10)	04.95 (9)	O(4)-Mn(2)-N(27)	88.32 (9)
O(3)′-Mn(1)-O(14)	161.05 (9)	O(8)-Mn(2)-O(12)	92.37 (9)
O(10)-Mn(1)-O(14)	93.98 (9)	O(8)-Mn(2)-N(16)	89.40 (9)
O(6)′-Mn(1)-O(3)′	94.32 (9)	O(8)-Mn(2)-N(27)	161.30 (9)
O(6)′-Mn(1)-O(10)	85.77 (9)	O(12)-Mn(2)-N(16)	99.24 (9)
O(6)′-Mn(1)-O(14)	86.13 (9)	O(12)-Mn(2)-N(27)	87.57 (9)
O(3)-Mn(2)-O(4)	86.30 (8)	N(16)-Mn(2)-N(27)	72.18 (10)

The distance of the μ_3-oxygen atoms above the Mn_4 plane is 0.592 Å. Each edge of the Mn_4 rhombus is bridged by either one or two μ_2-acetate groups; edges bridged by only one acetate have a slightly longer Mn···Mn separation (3.481 (1) Å) than those bridged by two acetate groups (3.288 (1) Å). The central Mn(1)···Mn(1)′ separation is significantly shorter (2.779 (1) Å) consistent with the two oxide bridges. Peripheral ligation is completed by two terminal bipy groups, one at each end of the molecule. The overall assembly possesses imposed C_i symmetry. As can be clearly seen in Figure 1, the molecule can be described as two Mn_3O triangular units fused along one edge. In discrete Mn_3O species, however, the μ_3-oxide lies in the Mn_3 plane and not above as in **1**. The average Mn oxidation level of +2.50 requires two Mn^{III} and two Mn^{II} centers; the former are assigned as the five-coordinate Mn(1) and Mn(1)′ atoms, while the latter are assigned as the six-coordinate Mn(2) and Mn(2)′ atoms. That Mn(2) and Mn(2)′ are in the +2 oxidation level is supported by (i) their Mn-ligand distances (2.103 (2)–2.267 (3) Å) which are longer than found for the Mn^{III} sites of complex **4** (vide infra) and (ii) the absence of a Jahn–Teller distortion characteristic of octahedral Mn^{III} (d^4). The five-coordinate Mn^{III} centers have distorted trigonal bipyramidal geometry with O(3)–Mn(1)–O(6)′ and O(3)′–Mn(1)′–O(6) (169.91 (9)°) representing the axes. Mn(1) and Mn(1)′ distances to their ligands (1.851 (2)–2.118 (2) Å) are shorter on average than those for Mn(2) and Mn(2)′ consistent with a higher oxidation state but also with the lower coordination number; thus, these distances by themselves were not sufficient evidence for assigning oxidation levels. Note also that the oxide bridges are not symmetrically disposed: Mn(1) and Mn(1)′ display significantly shorter Mn–O contacts (1.851 (2)–1.856 (2) Å) than Mn(2) and Mn(2)′ (2.103 (2) Å) consistent with a lower oxidation level in the latter. Finally, as will be discussed below, complex **4** contains an additional carboxylate bridging the central Mn_2 pair. Indeed, it is surprising that a similar situation is not found in **1**, for the resulting five-coordination at Mn(1) and Mn(1)′ is rare for this oxidation level with O,N-based ligation; octahedral coordination is by far the most common for Mn^{III}.

Complex **4** crystallizes in triclinic space group $P\bar{1}$ and contains well-separated anions and cations; the former and the disordered H_2O molecules will not be further discussed. The asymmetric unit contains a complete cation with no imposed symmetry. The molecule again possesses an Mn_4O_2 core which can be considered as two edge-sharing Mn_3O units, but the resulting arrangement does not have a planar Mn_4 moiety but instead a butterfly structure with Mn(1) and Mn(3) occupying the "hinge" sites and Mn(2) and Mn(4) occupying "wing-tip" sites. The molecule has idealized C_2 symmetry. As in **1**, either one or two μ_2-carboxylate groups bridge Mn–Mn edges, but now there is a seventh carboxylate

Table III. Selected Bond Distances (Å) and Angles (deg) for **4**

a. Bonds

Mn(1)···Mn(3)	2.848 (5)	Mn(2)···Mn(3)	3.371 (5)
Mn(1)···Mn(2)	3.312 (5)	Mn(2)···Mn(4)	5.593 (5)
Mn(1)···Mn(4)	3.385 (5)	Mn(3)···Mn(4)	3.299 (5)
Mn(1)-O(5)	1.918 (12)	Mn(3)-O(5)	1.889 (13)
Mn(1)-O(6)	1.911 (15)	Mn(3)-O(6)	1.930 (15)
Mn(1)-O(7)	1.939 (13)	Mn(3)-O(13)	1.956 (14)
Mn(1)-O(21)	1.937 (13)	Mn(3)-O(15)	1.970 (16)
Mn(1)-O(23)	2.184 (20)	Mn(3)-O(29)	2.202 (17)
Mn(1)-O(27)	2.188 (18)	Mn(3)-O(31)	2.259 (19)
Mn(2)-O(5)	1.844 (13)	Mn(4)-O(6)	1.804 (16)
Mn(2)-O(9)	2.144 (13)	Mn(4)-O(17)	2.197 (20)
Mn(2)-O(11)	2.157 (13)	Mn(4)-O(19)	2.171 (17)
Mn(2)-O(25)	1.865 (18)	Mn(4)-O(33)	1.914 (16)
Mn(2)-N(35)	2.052 (19)	Mn(4)-N(47)	2.084 (18)
Mn(2)-N(46)	2.076 (17)	Mn(4)-N(58)	2.021 (20)

b. Angles

Mn(1)-O(5)-Mn(2)	123.3 (7)	Mn(1)-O(6)-Mn(3)	95.7 (7)
Mn(1)-O(5)-Mn(3)	96.8 (6)	Mn(1)-O(6)-Mn(4)	131.3 (9)
Mn(2)-O(5)-Mn(3)	129.1 (7)	Mn(3)-O(6)-Mn(4)	124.0 (8)
O(5)-Mn(1)-O(6)	82.8 (6)	O(5)-Mn(3)-O(6)	83.1 (6)
O(5)-Mn(1)-O(7)	97.6 (7)	O(5)-Mn(3)-O(13)	94.7 (6)
O(5)-Mn(1)-O(21)	175.9 (7)	O(5)-Mn(3)-O(15)	172.6 (7)
O(5)-Mn(1)-O(23)	89.0 (6)	O(5)-Mn(3)-O(29)	87.2 (6)
O(5)-Mn(1)-O(27)	91.6 (6)	O(5)-Mn(3)-O(31)	99.5 (6)
O(6)-Mn(1)-O(7)	176.5 (7)	O(6)-Mn(3)-O(13)	176.7 (7)
O(6)-Mn(1)-O(21)	93.6 (6)	O(6)-Mn(3)-O(15)	96.4 (7)
O(6)-Mn(1)-O(23)	96.9 (6)	O(6)-Mn(3)-O(29)	90.0 (6)
O(6)-Mn(1)-O(27)	87.7 (6)	O(6)-Mn(3)-O(31)	87.9 (6)
O(7)-Mn(1)-O(21)	86.1 (6)	O(13)-Mn(3)-O(15)	86.1 (6)
O(7)-Mn(1)-O(23)	86.6 (6)	O(13)-Mn(3)-O(29)	92.4 (6)
O(7)-Mn(1)-O(27)	88.9 (7)	O(13)-Mn(3)-O(31)	90.0 (6)
O(21)-Mn(1)-O(23)	89.3 (6)	O(15)-Mn(3)-O(29)	85.4 (7)
O(21)-Mn(1)-O(27)	90.4 (6)	O(15)-Mn(3)-O(31)	87.8 (7)
O(23)-Mn(1)-O(27)	175.5 (6)	O(29)-Mn(3)-O(31)	172.6 (5)
O(5)-Mn(2)-O(9)	93.9 (5)	O(6)-Mn(4)-O(17)	95.1 (7)
O(5)-Mn(2)-O(11)	91.6 (5)	O(6)-Mn(4)-O(19)	92.0 (7)
O(5)-Mn(2)-O(25)	97.2 (7)	O(6)-Mn(4)-O(33)	98.5 (6)
O(5)-Mn(2)-N(35)	92.2 (7)	O(6)-Mn(4)-N(47)	92.5 (7)
O(5)-Mn(2)-N(46)	172.5 (8)	O(6)-Mn(4)-N(58)	172.1 (7)
O(9)-Mn(2)-O(11)	171.2 (6)	O(17)-Mn(4)-O(19)	168.3 (6)
O(9)-Mn(2)-O(25)	93.5 (6)	O(17)-Mn(4)-O(33)	92.0 (7)
O(9)-Mn(2)-N(35)	90.2 (6)	O(17)-Mn(4)-N(47)	86.7 (7)
O(9)-Mn(2)-N(46)	89.2 (6)	O(17)-Mn(4)-N(58)	85.8 (9)
O(11)-Mn(2)-O(25)	92.7 (6)	O(19)-Mn(4)-O(33)	96.1 (7)
O(11)-Mn(2)-N(35)	82.7 (6)	O(19)-Mn(4)-N(47)	83.7 (7)
O(11)-Mn(2)-N(46)	84.5 (6)	O(19)-Mn(4)-N(58)	85.9 (8)
O(25)-Mn(2)-N(35)	169.7 (6)	O(33)-Mn(4)-N(47)	169.0 (7)
O(25)-Mn(2)-N(46)	89.5 (8)	O(33)-Mn(4)-N(58)	89.4 (7)
N(35)-Mn(2)-N(46)	80.9 (7)	N(47)-Mn(4)-N(58)	79.7 (7)

bridging the two "hinge" atoms Mn(1) and Mn(3). Whether this is the cause or the effect of the difference in the two structures is uncertain. Two terminal bipy groups complete peripheral ligation with each of the four Mn^{III} atoms possessing distorted octahedral geometry. The two μ_3-oxide atoms O(5) and O(6) lie 0.351 and 0.318 Å below their respective Mn_3 planes and are thus on the same side of the molecule in contrast to **1**. The dispositions of the μ_3-oxides are much more symmetrical than in **1** and are consistent with all metals being in the same oxidation level. Indeed, differences are almost insigificant within the 3σ criterion, and, in fact, Mn(2)–O(5) and Mn(4)–O(6) distances (1.844 (13), 1.804 (16) Å) are now slightly shorter than those within the central Mn_2O_2 rhomb (1.889 (13)–1.930 (15) Å). The coordination around Mn(1) and Mn(3) shows clear evidence of a Jahn–Teller elongation, with O(23,27) and O(29,31) occupying axial positions; the situation at Mn(2) and Mn(4) is not as clear-cut, probably due to the greater variety of ligation types resulting from the terminal bipy groups, but a large range of distances (1.804 (16)–2.199 (20) Å) is nevertheless seen. Note, however, that Mn-ligand distances at the "wing-tip" positions are, on average, clearly shorter than those for atoms Mn(2) and Mn(2)′ of complex **1**, supporting the latter as Mn^{II} sites. Finally, the Mn···Mn separations again fall into two types; the Mn(1)···Mn(3) separation

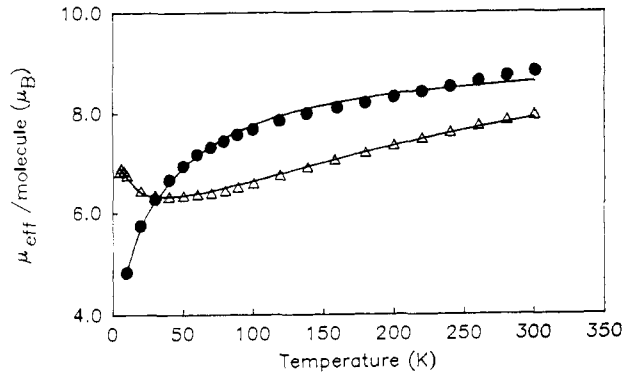

Figure 2. Plots of the effective magnetic moment, μ_{eff}, per Mn_4 molecule vs temperature for $[Mn_4O_2(O_2CMe)_6(bipy)_2]\cdot 2CHCl_3$ (**1**) (●) and $[Mn_4O_2(O_2CMe)_7(bipy)_2](ClO_4)\cdot 3H_2O$ (**4**) (△). The solid lines result from a least-squares fit of the data. See text for parameters.

(2.848 (5) Å) is significantly shorter than the remainder (3.299 (5)–3.385 (5) Å).

Complexes **1** and **4** represent the first structurally characterized examples of the $[Mn_4O_2]$ core, but several examples of $[Fe_4O_2]$-containing species have now been reported.[23-25] These all contain Fe^{III} and include $[Fe_4O_2(O_2CMe)_7(bipy)_2](ClO_4)$ which is similar to complex **4**.[25]

Magnetochemistry: Magnetic Susceptibility Studies. The solid-state, variable-temperature magnetic susceptibility of $[Mn_4O_2(O_2CMe)_6(bipy)_2]\cdot 2CHCl_3$ (**1**) and $[Mn_4O_2(O_2CMe)_7(bipy)_2](ClO_4)\cdot 3H_2O$ (**4**) were measured in the temperature range 5–300 K.

The effective magnetic moment per $Mn^{II}_2Mn^{III}_2$ cluster of complex **1** gradually decreases from 8.81 μ_B at 300.9 K to 4.86 μ_B at 10.0 K (Figure 2). The molar paramagnetic susceptibility increases with decreasing temperature over the whole range.

The general spin-Hamiltonian describing the isotropic exchange interaction for a tetranuclear complex is given by eq 5. The

$$H = -2(J_{12}S_1\cdot S_2 + J_{23}S_2\cdot S_3 + J_{34}S_3\cdot S_4 + J_{41}S_4\cdot S_1 + J_{13}S_1\cdot S_3 + J_{24}S_2\cdot S_4) \quad (5)$$

molecular structure of complex **1** (Figure 1) shows two central di-μ-oxo-bridged Mn^{III} ($S = 2$) ions with two other Mn^{II} ($S = 5/2$) ions connected to them through single μ-oxo bridges. The center of symmetry in the $[Mn_4O_2]^{6+}$ core indicates that the two central Mn^{III} ions are equivalent as are the two terminal Mn^{II} ions. The edge distances between Mn^{III} and Mn^{II} (3.288 and 3.488 Å) and bridging Mn^{III}–O–Mn^{II} angles (112.4°, 123.0°) are similar, while the distance between the Mn^{II} terminal ions (ca. 6 Å) is large. This suggests that the pairwise magnetic exchange interactions between pairs of Mn^{III} and Mn^{II} ions are nearly equivalent such that $J_{12} = J_{23} = J_{34} = J_{41} = J$ and that the coupling between the two terminal Mn^{II} is negligible and $J_{24} = 0$. This simplifies the spin-Hamiltonian (eq 5). Since $S_1 = S_3 = 2$ and $S_2 = S_4 = 5/2$ for the ions Mn(1), Mn(1′), Mn(2), and Mn(2′), respectively, this leads to eq 6.

$$H = -2J(S_1\cdot S_2 + S_2\cdot S_3 + S_3\cdot S_4 + S_4\cdot S_1) - 2J_{13}S_1\cdot S_3 \quad (6)$$

The eigenvalues of the spin-Hamiltonian (eq 6) may be determined by using the Kambe vector coupling method[26] with the following coupling scheme:

$$S_{13} = S_1 + S_3;\ S_{24} = S_2 + S_4;\ S_T = S_{13} + S_{24} \quad (7)$$

The energies of the spin states, which are eigenfunctions of the Hamiltonian in this coupling scheme, are given by eq 8. The

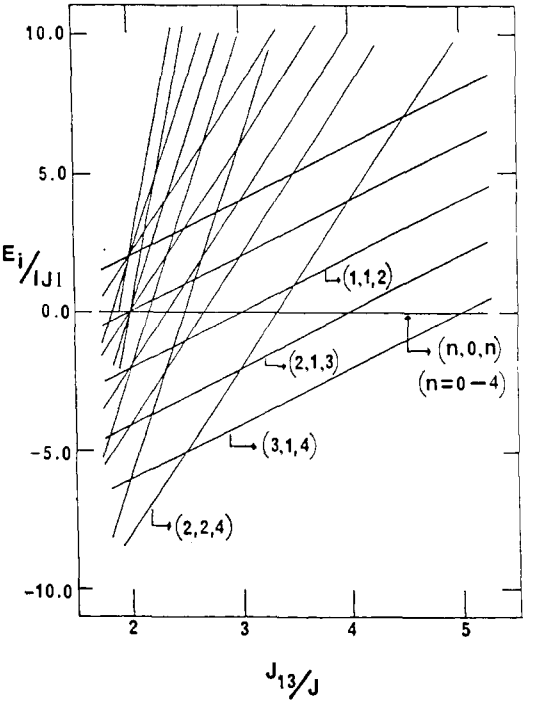

Figure 3. Ordering of the lowest energy states of a Mn^{III}_4 complex such as $[Mn_4O_2(O_2CMe)_7(bipy)_2](ClO_4)\cdot 3H_2O$ (**4**) as a function of the ratio of the exchange parameters J_{13}/J. The energy of the ith level is given in units of $|J|$. Equation 8 was used to calculate these energies. The label used to characterize each state is in the format (S_T, S_{13}, S_{24}), where S_T is the total spin for the state, S_{13} is the result of coupling the spin operators S_1 and s_3, and S_{24} results from coupling the spin operators S_2 and S_4.

overall degeneracy of this spin system is 900, made up of 110 individual spin states, ranging from $S_T = 0$–9.

$$E = -J[S_T(S_T + 1) - S_{13}(S_{13} + 1) - S_{24}(S_{24} + 1)] - J_{13}[S_{13}(S_{13} + 1)] \quad (8)$$

An expression for the molar paramagnetic susceptibility, χ_M, was derived for complex **1** by using the Van Vleck equation,[27] where an isotropic g tensor was assumed for the Zeeman Hamiltonian. This equation[51] was incorporated into a nonlinear, least-squares computer program[19] which was then used to fit the observed temperature dependence of the molar magnetic susceptibility as a function of the two exchange coupling parameters J and J_{13} and an isotropic g value. A good fit was found for $g = 1.70$, $J = -1.97$ cm^{-1}, and $J_{13} = -3.12$ cm^{-1} (Figure 2). The ground state calculated with these exchange coupling parameters and eq 8 is a quintet ($S_T = 2$) state. There are six other spin states within 15 cm^{-1} of the ground state.

The effective magnetic moment per Mn^{III}_4 cluster of complex **4** decreases with decreasing temperature from 7.96 μ_B at 300.6 K to a relatively constant value of 6.3–6.5 μ_B in the 90–20 K region and then increases slightly below 20 K (Figure 2). The spin-Hamiltonian of eq 6 can also be used to analyze the molar paramagnetic susceptibility of complex **4**, except that now $S_1 = S_2 = S_3 = S_4 = 2$, since all four manganese ions are Mn^{III}. The structure of complex **4** differs from **1** in the number of bridging acetate ligands between the metal ions. However, the overall geometry of the cluster is such that the μ-oxo exchange pathways connecting the central and terminal ions are very similar in their structural details (Mn–Mn 3.3–3.4 Å; Mn–O–Mn 123.3–131.90°). The energies of the spin states of complex **4** were used to calculate an expression for the molar paramagnetic susceptibility of this complex.[51] The molar paramagnetic susceptibility data for complex **4** were then fitted to this expression by using the least-squares fitting program. A good fit was obtained for $g = 2.0$, $J = -7.8$

(23) (a) Ponomarev, V. J.; Atovmyan, L. O.; Bobkova, S. A.; Turte, K. J. *Dokl. Acad. Nauk. SSSR* **1984**, *274*, 368. (b) Armstrong, W. H.; Roth, M. E.; Lippard, S. J. *J. Am. Chem. Soc.* **1987**, *109*, 6318.
(24) Murch, B. P.; Boyle, P. D.; Que, L., Jr. *J. Am. Chem. Soc.* **1985**, *107*, 6728.
(25) Vincent, J. B.; Huffman, J. C.; Christou, G., in preparation.
(26) Kambe, K. *J. Phys., Soc., Jpn.* **1950**, *5*, 48.
(27) Van Vleck, J. H. *The Theory of Electric and Magnetic Susceptibilities*; Oxford University Press: London, 1932.

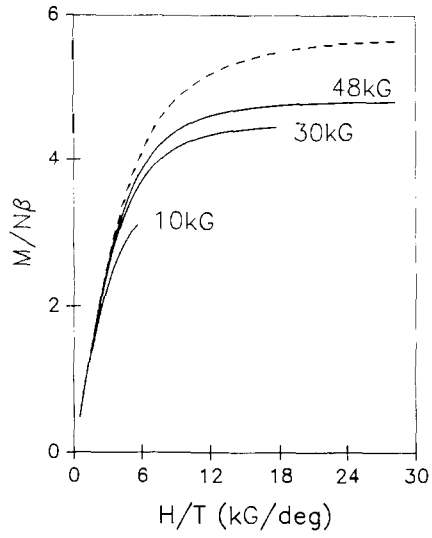

Figure 4. Plots of calculated reduced magnetization, $M/N\beta$, vs the ratio of the magnetic field over the absolute temperature, H/T. The dashed line corresponds to the Brillouin functionality expected for an isolated $S = 3$ state with $g = 1.9$ and no zero-field splitting. The solid lines were calculated for a $S = 3$ state experiencing an axial zero-field splitting (DS_z^2) with $D = +1.9$ cm^{-1} and $g = 1.9$.

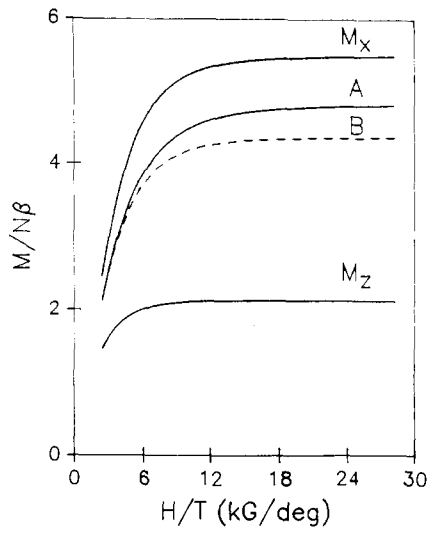

Figure 5. Plots of calculated reduced magnetization, $M/N\beta$, vs the ratio of the magnetic field over the absolute temperature, H/T. The perpendicular (M_X) and parallel (M_Z) components of the magnetization have been calculated for an $S = 3$ state with $D = +1.9$ cm^{-1} and $g = 1.9$. Curve A is a plot of $M/N\beta$ vs H/T calculated simply as the average of $M = {}^1/_3(2M_X + M_Z)$. Curve B is a plot of $M/N\beta$ vs H/T calculated as a true powder average of the magnetization for all orientations employing eq 10.

cm^{-1}, and $J_{13} = -23.5$ cm^{-1} (Figure 2). The ground state for these exchange parameters is a septet $S_T = 3$ state with two excited quintet states at about 15 cm^{-1} and five excited $S_T = 4, 3, 2, 1, 0$ states at about 30 cm^{-1} above the $S_T = 3$ state. This arrangement of states explains the relatively constant value of the magnetic moment in the 20–90 K region, and the increase at lower temperatures as the $S_T = 3$ state becomes the only populated state at the lowest temperatures. Figure 3 gives a plot of the energies in units of $|J|$ of the lowest energy states for the Mn^{III}_4 complex **4** as a function of the ratio J_{13}/J. It can be seen that only when the value of J_{13}/J is between 4.9 and 2.5 is the ground state characterized by $(S_T, S_{13}, S_{24}) = (3, 1, 4)$. When $J_{13}/J > 4.9$, then five energetically degenerate states, $(S_T, S_{13}, S_{24}) = (n, 0, n)$ with $n = 0$–4, become the ground state with the (3, 1, 4) state as the lowest lying excited state. If $J_{13}/J < 2.5$, then the quintet state (2, 2, 4) becomes the ground state.

The effective magnetic moment per $Mn^{II}Mn^{III}_3$ for complex **2** decreases monotonically with temperature from 8.29 μ_B at 300.7 K to 5.08 μ_B at 5.0 K (not shown). Fitting of the data to a theoretical expression for the susceptibility versus temperature behavior is postponed until such time as the crystal structure of complex **2** is obtained. This will allow identification of the position of the Mn^{II} ion and derivation of the appropriate expression.

Magnetochemistry: Magnetization Versus Magnetic Field Studies. Least-squares fitting of the magnetic susceptibility data for complexes **1** and **4** in terms of the above magnetic exchange coupling models indicates that there are several spin states close to the ground states in these two complexes. Bulk magnetization measurements were performed in the temperature range 1.7 to 15 K in fields of 10, 30, or 48 kG to confirm the nature and ordering of the low-energy states predicted from the susceptibility studies.

In the case of a molecule such as complex **4** which has as a ground state an isolated spin multiplet, the variation of the magnetization with H/T would follow that predicted by the appropriate Brillouin function.[28] The dashed line in Figure 4 shows the Brillouin function for $S = 3$ with $g = 1.9$. However, if there is an additional splitting of the multiplet due to contributions from single-ion, zero-field splitting, then the isothermal or isofield curves for varying field or temperature, respectively, do not superimpose. In Figure 4, the solid lines have been calculated for a $S = 3$ state, experiencing axial zero-field splitting DS_z^2 with $D = +1.9$ cm^{-1} and $g = 1.9$. It can be seen that the isofield lines at 10, 30, and 48 kG do not superimpose due to the zero-field splitting. This nonsuperimposability of isofield lines is due to the differing populations of the components of the zero-field-split ground state as the orientation of the magnetic field is varied with respect to the molecule.

The magnetization for such a system may be calculated by using the basic thermodynamic relation[29] given in eq 9. This equation

$$M = N\sum_{i=1}^{P}\left(-\frac{\delta E_i}{\delta H}\right)\exp(-E_i/kT)/\sum_{i=1}^{P}\exp(-E_i/kT) \quad (9)$$

reduces to the Brillouin function in the case of no zero-field splitting. If there is zero-field splitting,[30] then the calculated magnetization becomes anisotropic. In Figure 5 are shown the M_z and M_x components of the magnetization for a $S = 3$ ground state with axial zero-field splitting characterized by $D = +1.9$ cm^{-1} and $g = 1.9$. To obtain the powder value of the magnetization for a polycrystalline sample, a suitable averaging of the magnetization must be carried out. In the case of low magnetic fields and high temperatures where the magnetization is a linear function of H, this entails simply numerically averaging the three principal values M_x, M_y, and M_z. In the region of high fields and low temperatures, a true powder average of the magnetization for all orientations must be made[31,32] using eq 10. In eq 10, θ,ϕ are the

$$\bar{M} = \frac{-N}{4\pi}\int_{\theta=0}^{\pi}\int_{\phi=0}^{2\pi}\left[\sum_{i=1}^{P}\left(\frac{\delta E_i}{\delta H}\right)\exp(-E_i/kT)/\sum_{i=1}^{P}\exp(-E_i/kT)\right]\sin\theta\,d\theta\,d\phi \quad (10)$$

polar angle orientations of the field with respect to the molecular principal axis system, N is Avogadro's number, and $\delta E_i/\delta H$ is the change in the energy of the ith level in response to a change in a magnetic field. In general, the energies of the various spin sublevels are obtained by diagonalization of the Hamiltonian matrix, including the Zeeman terms, and the derivatives of the energy with respect to the magnetic field are calculated from the corresponding eigenvectors by using the Hellman–Feynman

(28) Carlin, R. L. *Magnetochemistry*; Springer-Verlag: Berlin, 1986.

(29) Vermaas, A.; Groeneveld, W. L. *Chem. Phys. Lett.* **1974**, *27*, 583.
(30) Kennedy, B. J.; Murray, K. S. *Inorg. Chem.* **1985**, *24*, 1552.
(31) Boyd, P. D. W.; Martin, R. L. *J. Chem. Soc., Dalton Trans.* **1979**, 92.
(32) Gerloch, M.; McMeeking, R. F. *J. Chem. Soc., Dalton Trans.* **1975**, 2443.

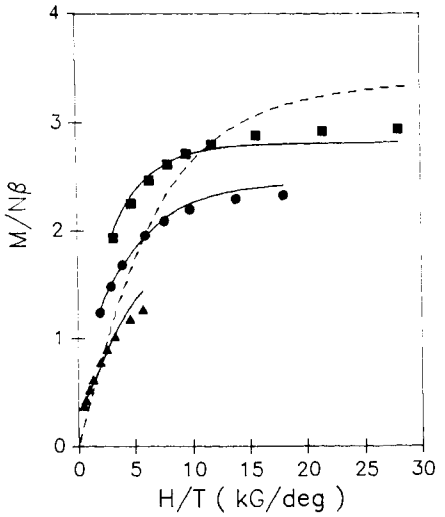

Figure 6. Plots of reduced magnetization, $M/N\beta$, vs the ratio of H/T for $[Mn_4O_2(O_2CMe)_6(bipy)_2]\cdot 2CHCl_3$ (**1**) at three magnetic fields: ▲, 10 kG; ●, 30 kG; and ■, 48 kG. The three solid lines result from least-squares fitting of the $M/N\beta$ vs H/T data for **1** to the powder average eq 10, where the energies of all states (E_i) for complex **1** were determined by eq 8. See text for least-squares fitting parameters.

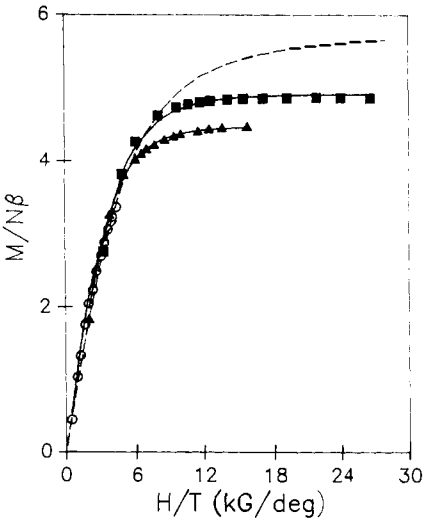

Figure 7. Plots of reduced magnetization, $M/N\beta$, vs the ratio of H/T for $[Mn_4O_2(O_2CMe)_7(bipy)_2](ClO_4)\cdot 3H_2O$ (**4**) at three magnetic fields: ○, 10 kG; ▲, 30 kG; and ■, 48 kG. The three solid lines result from least-squares fitting of the $M/N\beta$ vs H/T data for complex **4** to the powder average eq 10, where the energies of all states (E_i) for complex **4** were determined by eq 8. See text for least-squares fitting parameters.

theorem.[31,32] The integral in eq 10 is evaluated numerically. Figure 5 shows a comparison of the two averaging methods in the calculation of the reduced magnetization $M/N\beta$ for a $S = 3$ state with $D = +1.9$ cm^{-1} and $g = 1.9$. Dashed line B results from the simple average of components, i.e., $M = {}^1/_3(M_z + 2M_x)$. The solid line A results from a complete powder average using eq 10. At low fields and/or high temperatures, lines A and B coalesce since the two types of calculations then give the same result. However, at high fields and/or low temperatures, there is a divergence, and only the powder average is correct.

The bulk reduced magnetization for complex **1** ($M/N\beta$ where β is the Bohr magneton) is shown in Figure 6 plotted as a function of H/T. It can be seen that the three isofield magnetization curves deviate from that expected for an isolated $S = 2$ ground state with no zero-field splitting. The dashed line in Figure 6 was calculated with the Brillioun function for an $S = 2$ state with $g = 1.70$. The three isofield magnetization data sets at 10, 30, and 48 kG were first least-squares fit to eq 10 with the energy of each spin state, E_i, determined by eq 8. This least-squares fitting gave parameters of $g = 1.87$, $J = -2.30$ cm^{-1}, and $J_{13} = -3.05$ cm^{-1}. However, an improved fit of the data to eq 10 could be found not only by including all spin states at the energies specified by the Kambe model but also by allowing for axial zero-field splitting in the $S = 2$ ground state. This second fit gave parameters of $g = 1.70$, $J = -1.98$ cm^{-1}, and $J_{13} = -3.12$ cm^{-1} and a value of $D = -1.93$ cm^{-1} for the $S = 2$ ground state. The solid lines in Figure 6 illustrate how well this fit agrees with the experimental data. The fitting procedure employed spatial averaging of the magnetization for data below 10 K and averaging of the principal values of the magnetization for data above 10 K.[31,32] It was gratifying that the exchange parameters obtained from fitting the magnetization data are in good agreement with those obtained above. This provides independent confirmation of the lower energy spin-state distribution for complex **1**.

In contrast to the case for complex **1**, the ground state predicted for complex **4** from the susceptibility data fitting is an $S = 3$ ground state separated by greater than 15 cm^{-1} from the lowest energy excited state. The reduced magnetization versus H/T data for complex **4** (Figure 7) at the highest field studied saturates at a value of about $M/N_\beta \leq 5$. This is obviously less than the $M/N_\beta = 6$ value expected for a septet ($S = 3$) state with $g = 2.0$. The dashed line in Figure 4 illustrates what is expected for an $S = 3$ state with no zero-field splitting. An attempt was first made to least-squares fit the three isofield data sets for complex **4** to eq 10 for an isolated $S = 3$ state with only axial zero-field splitting (DS_z^2). This fit agreed with the data only moderately well. A second fit was tried for an isolated $S = 3$ state with both axial and rhombic $E(S_x^2 - S_y^2)$ zero-field splitting. The three solid lines in Figure 7 result from this fit and can be seen to agree well with the data. The third theoretical line corresponding to the 10 kG (○) isofield data set is somewhat obscured in Figure 7. This fit gave parameters of $g = 1.90$, $D = +1.90$ cm^{-1}, and $E = +0.32$ cm^{-1}.

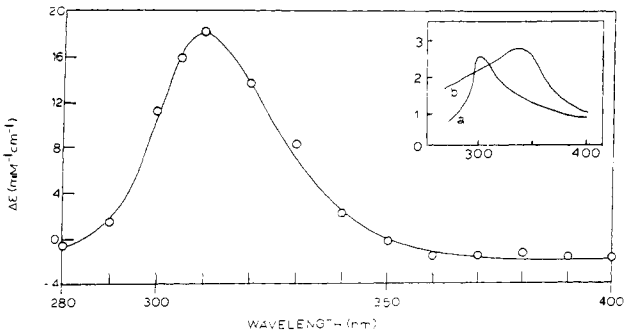

Figure 8. Electronic difference spectrum in CH_2Cl_2 for the $[Mn_4O_2(O_2CPh)_7(bipy)_2]^{0,+}$ pair (complexes **2** and **9**). The inset is the corresponding spectra for (a) the $S_0 \rightarrow S_1$ and (b) the $S_1 \rightarrow S_2$ and $S_2 \rightarrow S_3$ transitions.

Magnetostructural Commentary. The most significant feature in a comparison of the exchange coupling parameters between complexes **1** and **4** is the variation by nearly an order of magnitude in the coupling between the two central di-μ-oxo-bridged Mn^{III} ions in these two complexes where $J_{13} = -3.12$ cm^{-1} for complex **1** and -23.5 cm^{-1} for complex **4**. A comparison with such Mn^{III}–Mn^{III} interactions in the recently reported hexanuclear[33] and nonanuclear[34] complexes containing these same central bridging units suggests the larger value of J_{13} for complex **4** is quite reasonable. An explanation of this variation between **1** and **4** may be seen in a comparison of the details of the structure of the $[Mn_4O_2]$ units in **1**, **4**, and the hexanuclear and nonanuclear Mn complexes. All contain two octahedrally coordinated Mn^{III} ions sharing an edge comprised of two μ-oxide ions. The bond angles and bond lengths in these units are all similar (Table IV). The two longest bond lengths for each Mn^{III} ion in complex **4** are trans oxygen atoms of bridging acetates, suggesting a Jahn–Teller

(33) Schake, A. R.; Vincent, J. B.; Li, Q.; Boyd, P. D. W.; Folting, K.; Huffman, J. C.; Hendrickson, D. N.; Christou, G. *Inorg. Chem.*, in press.
(34) Christmas, C.; Vincent, J. B.; Chang, H.-R.; Huffman, J. C.; Christou, G.; Hendrickson, D. N. *J. Am. Chem. Soc.* **1988**, *110*, 823.

Table IV. Exchange Coupling Constants and μ-Oxo-Bridging Angles in Polynuclear Manganese Complexes[a]

complex	ox state	J (cm^{-1})	Mn-O-Mn (deg)	Mn-O (Å)
1[b]	II-III	-1.97[m]	112.4, 123.0	1.851-2.103
	III-III	-3.12[l]	97.12	1.851, 1.856
4[b]	III-III	-7.80[m]	123.3-131.3	1.804-1.930
	III-III	-23.53[l]	95.7, 96.8	1.889-1.930
$Mn_6O_2(O_2CPh)_{10}(py)_2(MeCN)_2$[c]	II-III	-0.8[m]	88.1-119.6	2.183-2.220
	III-III	-42.0[l]	96.2, 97.2	1.874-1.895
	II-II	-2.4[m]	117.4, 119.9	2.183-2.220
$Mn_9O_4(O_2CPh)_8(sal)_8(salH)_2(py)_4$[d]	II-III	-0.97[m]	108.3-136.1	1.976-2.385
	III-III	-26.2[l]	96.4, 96.9	1.878-1.896
	III-III	-11.2[m]	129.4-133.1	1.872-1.896
$[Mn_2(bpmp)(O_2CMe)_2](ClO_4)_2$[e]	II-III	-6.0[m]	114.4	2.19, 1.90
$Mn_2(bcmp)(O_2CMe)_2](ClO_4)_2$[e]	II-III	-7.7[m]	112.1	2.17, 1.96
$Mn_3O(O_2CMe)_6(py)_3\cdot py$[f]	II-III	-5.1[m]	120.0	1.936
	III-III	-8.3[m]	120.0	1.936
$Mn_2(bipy)_2(biphen)_2(biphenH)$[g]	II-III	+0.89[l]	97.1, 102.4	2.142, 2.112
$[LMn_2Cl_2Br]\cdot H_2O$[h]	II-III	-1.7[l]	102.5, 93.6	1.931-2.386
$[LMn_2Br_3]\cdot{}^1/_2CH_2Cl_2$[h]	II-III	-1.0[l]		
$Mn_2O(O_2CMe)_2(bipy)_2Cl_2$[i]	III-III	-4.1[m]	124.3	1.777, 1.788
$Mn_2O(O_2CMe)_2(bipy)_2(N_3)_2$[i]	III-III	+3.4[m]	122.0	1.802
$Mn_2O(O_2CMe)_2(HB(pz)_3)_2$[j]	III-III	-0.2 to -0.7[m]	125.1	1.773
$[L'_2Mn_2O(O_2CMe)_2](ClO_4)_2$[k]	III-III	+9[m]	120.9	1.81

[a] Abbreviations: $salH_2$ = salicylic acid, $biphenH_2$ = 2,2'-biphenol; bcmp is the same as bpmp (see ref 37) except that each of the bis(pyridylmethyl)amine units are replaced by 1,4,7-triazacyclononane units; LH_2 = Schiff-base condensation product of 1,3-diaminopropane and 2,6-diformyl-4-*tert*-butylphenol; $HB(pz)_3^-$ = hydrotris(1-pyrazolyl)borate; L' = 1,4,7-trimethyl-1,4,7-triazacyclononane. [b] This work. [c] Reference 33. [d] Reference 34. [e] Reference 35. [f] Reference 16. [g] Reference 36. [h] Reference 37. [i] Reference 38. [j] Reference 20. [k] Reference 39. [l] Di-μ-oxo bridge. [m] Mono-μ-oxo bridge.

distortion along these axes (identified as z). The four unpaired electrons of each Mn atom in the xz, yz, xy, and z^2 orbitals are available to become involved in spin–spin exchange coupling pathways. Antiferromagnetic π pathways are available between xz, yz pairs (one orbital on each metal) via the p orbitals of the bridging oxygen atoms and antiferromagnetic σ pathways between xy pairs via oxygen s and p orbitals. The Mn z^2 electrons may interact via a ferromagnetic pathway involving an orthogonality at the bridging oxygen atom. A net antiferromagnetic interaction is found as expected.

In contrast, the central Mn ions in complex **1** are five-coordinate with approximate trigonal bipyramidal coordination about each Mn. The 3-fold axis of this trigonal bipyramid is directed along one of the bridging Mn–O bonds. The unpaired electrons of each Mn ion would occupy xz, yz, xy, and x^2-y^2 orbitals. No strong antiferromagnetic σ pathways are possible for this bridging arrangement, and the small magnitude of the coupling in complex **1** reflects this.

The Mn^{II}–Mn^{III} interactions obtained in this work for complexes **1** and **2** are small, as has been found in most such molecules that have been reported to have such a Mn^{II}–Mn^{III} interaction (Table IV).

Electron Paramagnetic Resonance. No EPR signals could be seen for the Mn^{III}_4 complex **4**, even at liquid-helium temperatures.

EPR spectra at both X- and Q-band frequencies were run for a polycrystalline sample of $[Mn_4O_2(O_2CMe)_6(bipy)_2]\cdot 2CHCl_3$ (**1**). Many fine structure features are seen; a figure is available in the Supplementary Material. Frozen glass (CH_2Cl_2/toluene) X-band spectra for complex **2** were run at 7.5, 15, and 30 K. The spectra exhibit two signals, one at $g \sim 4$ and one hyperfine structured signal at $g \sim 2$. The relative intensities of the two signals do not change appreciably in the 7.5–30 K range. Further discussion and interpretation of the EPR properties of complex **2** are again postponed until the structure and electronic makeup of this molecule have been elucidated.

Electronic Difference Spectroscopy. The metal oxidation levels at the various S_n levels of the water oxidation site remain to be unambiguously elucidated. A fitting of the various EPR data available has led to the conclusion that three separate assignments are possible,[40] as reproduced in Table V. There seems to have been a general preference for assignments B or C in many literature discussions, based on the particular data being interpreted. Use of electronic difference spectra for the various S_n states has been proving of some utility in attempts to distinguish the possibilities. Dekker et al. reported that each $S_n \rightarrow S_{n+1}$ transition

Table V. Possible Manganese Oxidation States in the S_n Levels, Assuming Tetranuclearity

S_n	A	B	C
S_0	$3Mn^{II}$, Mn^{III}	Mn^{II}, $3Mn^{III}$	$3Mn^{III}$, Mn^{IV}
S_1	$2Mn^{II}$, $2Mn^{III}$	$4Mn^{III}$	$2Mn^{III}$, $2Mn^{IV}$
S_2	Mn^{II}, $3Mn^{III}$	$3Mn^{III}$, Mn^{IV}	Mn^{III}, $3Mn^{IV}$
S_3	$4Mn^{III}$	$2Mn^{III}$, $2Mn^{IV}$	$4Mn^{IV}$

displayed an identical difference spectrum, suggesting that each advancement entailed the same $Mn^{x+} \rightarrow Mn^{(x+1)+}$ oxidation to be occurring.[41] By comparison with Mn gluconate spectra, they concluded that this was a $Mn^{III} \rightarrow Mn^{IV}$ transition favoring assignment C. We subsequently showed that the difference spectrum for the isostructural $[Mn_3O(O_2CMe)_6(py)_3]^{0,+}$ complexes, containing Mn^{II}, $2Mn^{III}$, and $3Mn^{III}$, respectively, looked similar to those of the native site, suggesting a $Mn^{II} \rightarrow Mn^{III}$ transition might also be involved in the latter.[14] More recent work,[42] using NH_2OH-treated chloroplast particles, has established that the difference spectrum for the $S_1 \rightarrow S_2$ and $S_2 \rightarrow S_3$ transitions are identical but different from that of the $S_0 \rightarrow S_1$ transition. They interpreted their results as indicating $S_0 \rightarrow S_1$ to involve a $Mn^{II} \rightarrow Mn^{III}$ transition and $S_1 \rightarrow S_2$ and $S_2 \rightarrow S_3$ to involve a $Mn^{III} \rightarrow Mn^{IV}$ transition, thus supporting assignment B.

As an extension to our earlier work, we have now investigated the difference spectrum for the $[Mn_4O_2(O_2CPh)_7(bipy)_2]^{0,+}$ pair, complexes **2** and **9**, respectively. The spectrum is reproduced in

(35) Diril, H.; Chang, H.-R.; Larsen, S. K.; Potenza, J. A.; Pierpont, C. G.; Schugar, H. J.; Isied, S. S.; Hendrickson, D. N. *J. Am. Chem. Soc.* **1987**, *109*, 6207.
(36) Bashkin, J. S.; Schake, A. R.; Vincent, J. B.; Chang, H.-R.; Huffman, J. C.; Christou, G.; Hendrickson, D. N. *J. Chem. Soc., Chem. Commun.* **1988**, 700.
(37) Chang, H.-R.; Larsen, S. K.; Boyd, P. D. W.; Pierpont, C. G.; Hendrickson, D. N. *J. Am. Chem. Soc.* **1988**, *110*, 4565.
(38) Vincent, J. B.; Li, Q.; Boyd, P. D. W.; Folting, K.; Huffman, J. C.; Hendrickson, D. N.; Christou, G., submitted for publication.
(39) Wieghardt, K.; Bossek, U.; Ventur, D.; Weiss, J. *J. Chem. Soc., Chem. Commun.* **1985**, 347. Koppen, M.; Fresen, G.; Weighardt, K.; Llusen, R.; Nuber, B. *Inorg. Chem.* **1988**, *27*, 721.
(40) de Paula, J. C.; Beck, W. F.; Brudvig, G. W. *J. Am. Chem. Soc.* **1986**, *108*, 4002.
(41) (a) Dekker, J. P.; Van Gorkom, H. J.; Wensink, J.; Ouwehand, L. *Biochim. Biophys. Acta* **1984**, *767*, 1. (b) Dekker, J. P.; Van Gorkom, H. J.; Brok, M.; Ouwehand, L. *Biochim. Biophys. Acta* **1984**, *764*, 301.
(42) (a) Witt, H. T.; Schluder, E.; Brettel, K.; Saygin, O. *Photosyn. Res.* **1986**, *9*, 1453. (b) Kretschmann, H.; Dekker, J. P.; Saygin, O.; Witt, H. T. *Biochim. Biophys. Acta* **1988**, *932*, 358.

Table VI. Proton NMR Data in $CDCl_3$ Solution at 23 °C

$[Mn_4O_2(O_2CR)_7(4,4'\text{-}X_2\text{-bipy})_2]^+$	ligand	shifts[a]
R = CH_3, X = H (**4**)	O_2CR	44.9, 36.4, 27.8, 22.6[b]
	bipy[c]	-130.8 (6), 20.1 (5), -29.9 (4), 33.0 (3)
		-76.2 (6'), -19.7 (5'), -18.7 (4'), -11.4 (3')
R = CD_3, X = H	O_2CR	
	bipy	-132.2 (6), 20.1 (5), -29.8 (4), 33.0 (3)
		-75.6 (6'), -19.1 (5'), -18.6 (4'), -11.4 (3')
R = CH_3, X = Me (**5**)	O_2CR	43.7, 35.2, 26.7, 21.6[b]
	bipy	-130.6 (6), 20.0 (5), 42.1 (Me), -31.3 (3)
		-82.8 (6'), -19.1 (5'), 32.2 (Me), -14.0 (3')

[a] Data are chemical shifts in ppm from TMS; downfield shifts are designated as positive. [b] Unique acetate bridging the "hinge" Mn atoms. [c] Numbers in parentheses refer to the bipy ring positions; the primed positions belong to the ring cis to the μ_3-oxide atoms.

Figure 8, where the spectra of Witt et al. are also reproduced as an inset. As can be seen, the difference spectrum of the synthetic complexes bears a striking similarity to the $S_0 \rightarrow S_1$ spectrum, both in overall profile and peak position (~310 nm). We are led to conclude that the $S_0 \rightarrow S_1$ transition may indeed represent a $Mn^{II} \rightarrow Mn^{III}$ oxidation, in agreement with the conclusion by Witt et al. and supporting assignment B. In the absence of a $[Mn_4O_2(O_2CPh)_7(bipy)_2]^{2+}$ complex, containing $3Mn^{III}$, Mn^{IV}, we cannot determine the corresponding spectrum for the $Mn^{III} \rightarrow Mn^{IV}$ transition, but one might certainly be expected to predict this as being at lower energies, consistent with the $S_1 \rightarrow S_2$ and $S_2 \rightarrow S_3$ spectra. In summary, difference spectra cannot by themselves be definitive but do, nevertheless, suggest assignment B to be probably correct based on available data.

Proton NMR Spectroscopy. To determine the feasibility of using proton NMR as an additional technique for the characterization of tetranuclear $[Mn_4O_2]$ complexes, an NMR investigation has been carried out on complex **4**. The complex has a large effective magnetic moment at room temperature but, nevertheless, this spin-even Mn^{III} system has been found to display well-resolved spectra in which all expected resonances for the different protons have been located. In $CDCl_3$, 12 ligand resonances are clearly observed in the range ~+50 to −150 ppm. (A figure is available in the Supplementary Material.) Assuming effective C_2 symmetry for the cation in solution, these resonances correspond exactly to the 12 expected: one from each of four inequivalent types of $MeCOO^-$ groups and eight from bipy ring protons which are all inequivalent under C_2 symmetry. Inversely, this supports retention of the tetranuclear structure of **4** in solution.

The assignments in Table VI of the various resonances was accomplished by a combination of the following: (i) preparation of the deuterio-acetate derivative of **4** which allowed ready identification of the four acetate peaks; (ii) consideration of peak widths which readily allowed assignment of the bipy 6 and 6' protons that are very broad as a consequence of their proximity to Mn atoms; and (iii) preparation of the 4,4'-Me_2-bipy derivative (complex **5**) which identified the bipy 4 and 4' protons. The four acetate resonances occur at 44.9, 36.4, 27.8, and 22.6 ppm in relative intensities of ~2:2:2:1, respectively. This clearly identifies the 22.6-ppm peak as being due to the unique acetate group bridging the "hinge" Mn atoms Mn(1) and Mn(3). Assignment of the other three resonances to particular groups cannot be made unambiguously and is not attempted at this time. The remaining resonances due to the bipy protons occur over a remarkably large range of ~175 ppm. The very broad resonances at the extreme upfield region are readily assigned as the 6,6' protons. The upfield resonances at −18.7 and −29.9 are due to the 4.4' protons, since they are absent in complex **5** and are also the sharpest of the eight, being furthest from the Mn atoms. The 4,4'-Me resonances in **5** are downfield of their diamagnetic position, and this change in sign between the isotropic shifts of the H and Me protons at the 4,4' positions is clear evidence of a π spin-delocalization mechanism dominating the observed shifts at these positions. Indeed, Wicholas and Drago[43] have demonstrated that π-delocalization is likely the sole component responsible for the contact shifts at the 4,4' positions of the bipy molecule; any σ-delocalization contribution to the shifts would be very attenuated at these large distances from the paramagnetic center.

If it is assumed that the d_{z^2} orbital of a "wing-tip" Mn atom is oriented along the short Mn-oxide bond, then this orbital becomes destabilized above the $d_{x^2-y^2}$ orbital in energy and is thus unoccupied. The pyridine ring disposed trans to the oxide ligand would consequently be expected to be influenced, to a first approximation, by only a π spin-delocalization pathway from occupied metal d_π orbitals (neglecting dipolar effects); in contrast, the pyridine ring cis to the oxide would be expected to be influenced by both σ and π spin-delocalization pathways from the metal $d_{x^2-y^2}$ and d_π orbitals, respectively. Pursuing this thinking further, then the large difference in the observed resonance positions of the 6,6'-protons (54.6 ppm) can be rationalized. The proton (6') of the pyridine ring cis to the oxide is contact shifted downfield relative to the proton of the trans ring by a σ spin-delocalization mechanism. The remaining four bipy resonances are assigned somewhat more tentatively. The two peaks at −11.4 and 33.0 ppm are assigned to the 3,3' protons, and the peaks at −19.1 and 20.1 ppm are assigned to the 5,5' protons; the former are slightly broader, consistent with their closer proximity to the Mn centers. Specific assignment of each resonance to a particular proton is difficult, and the complete assignments in Table VI are based on comparisons with other transition-metal bipy complexes[43-45] and related tris(1-pyrazolyl)borate species.[20] We are unaware of any NMR studies on other metal bipy complexes for comparison containing similarly inequivalent pyridine rings.

In summary, all resonances due to ligand protons in complex **4** have been located and are well-resolved. Firm identification of bipy and acetate protons is possible, although each resonance cannot be unambiguously assigned to a particular proton in every case. The pattern of isotropic shifts is indicative of both σ and π spin-delocalization mechanisms to be operating in the complete molecule. With this preliminary utility of NMR for the study of $[Mn_4O_2]$ species established, more extensive studies are planned, including use of other materials available to us, anticipating that NMR may prove a useful addition to the arsenal of techniques available for comparative studies between Mn biomolecules and their synthetic models.

Electrochemistry. A cyclic voltammogram (CV) of complex **9** in CH_2Cl_2 displayed two quasi-reversible processes, a reduction to complex **2** at $E_{1/2}$ = −0.16 V vs ferrocene (Fc), and an oxidation to the $Mn^{III}_3Mn^{IV}$ level at $E_{1/2}$ = +0.87 V. For both processes, a plot of i_p vs $\nu^{1/2}$ gave a straight line in the scan rate (ν) range of 50–1000 mV/s. The CV of complex **2** displayed the same two features at the same potentials, both now being oxidations; this is further support for the identity of complex **2**. Additionally, complexes **2** and **9** both displayed an irreversible reduction with E_c = 1.01 V at 100 mV/S. These processes are summarized below.

$$[Mn_4O_2(O_2CPh)_7(bipy)_2]^- \xleftarrow{-1.01\ V} \underset{2Mn^{II},2Mn^{III}}{}$$

$$[Mn_4O_2(O_2CPh)_7(bipy)_2]^0 \underset{}{\overset{-0.16\ V}{\rightleftharpoons}} \underset{Mn^{II},3Mn^{III}}{\mathbf{2}}$$

$$[Mn_4O_2(O_2CPh)_7(bipy)_2]^+ \overset{+0.87\ V}{\rightleftharpoons} \underset{4Mn^{III}}{\mathbf{9}}$$

$$\underset{3Mn^{III},Mn^{IV}}{[Mn_4O_2(O_2CPh)_7(bipy)_2]^{2+}}$$

(43) Wicholas, M.; Drago, R. S. *J. Am. Chem. Soc.* **1968**, *90*, 6946.
(44) De Simone, R. E.; Drago, R. S. *J. Am. Chem. Soc.* **1970**, *92*, 2343.
(45) Horrocks, W. deW., Jr. In *NMR of Paramagnetic Molecules*; LaMar, G. N., Horrocks, W. deW., Jr., Holm, R. H., Eds.; Academic Press: New York, 1973; p 127.

Table VII. Comparison of Complex **4** with EXAFS Data on S_1

species	short Mn···Mn, Å	n	long Mn···Mn, Å	n	Mn–O, Å	n	Mn–L, Å	n
S_1	2.69 (3)	0.68	approx 3.3 Å		1.76 (3)	2.27	1.98 (3)	3.25
4	2.848 (5)	0.5	3.299 (5)–3.385 (5)	2.0	1.83 (4)	1.50	2.07 (12)	4.50

Similar quasi-reversible behavior has been seen for the dinuclear complexes $[Mn_2O(OAc)_2(TACN)_2]^{2+}$ (TACN = 1,4,7-triazacyclononane)[39] and $Mn_2O(OAc)_2(HB(pz)_3)_2$.[20] The former complex in MeCN displayed a quasi-reversible oxidation at +0.59 V to the $Mn^{III,IV}_2$ compound which was subsequently generated chemically and structurally characterized. The latter complex exhibited two quasi-reversible oxidations to give the $Mn^{III,IV}_2$ and $Mn^{IV,IV}_2$ complexes at $E_{1/2}$ = +0.51 and 1.22 V, respectively. Thus, this family of Mn complexes with mixed oxide, carboxylate, and amine ligation all appear to exhibit fairly slow rates of heterogeneous electron transfer.

Complex **7** also displays a quasi-reversible oxidation in CH_2Cl_2 with $E_{1/2}$ = −0.02 V vs Fc. A remarkable influence of removing one carboxylate is, therefore, apparent. This suggests that it may prove possible to synthesize a complex containing a cation of formulation $[Mn_4O_2(O_2CR)_6(bipy)_2]^+$, but we have only encountered complexes **2** and **3** at this oxidation level to date.

The combined results of our electrochemical studies demonstrate that the $[Mn_4O_2]^{n+}$ core is capable of attaining four interconvertible oxidation levles (n = 6–9) although the n = 6 level appears stable only with six carboxylate ligands.

Biological Significance. The successful attainment of tetranuclear Mn complexes with oxide bridges and peripheral O,N-based ligation begs the overall question of how closely they might correspond to the native Mn site of the water oxidation center should it prove to be tetranuclear.[3,40,47] In the present absence of structural data on the latter, recourse must be made for comparison purposes to available EPR[40,46,47] and extended X-ray absorption fine structure (EXAFS)[48] data on the native site. Taking the EPR-active S_2 state to possess $3Mn^{III}$, Mn^{IV}, S_1 must contain $4Mn^{III}$, and, on this basis, the EXAFS fits for S_1 are compared in Table VII with structural parameters obtained from the crystal structure of complex **4**. The best fit parameters obtained from the Mn K-edge EXAFS data on S_1 indicate that each Mn is coordinated to 3.25 N or O ligand atoms at a distance of approximately 1.98 Å, 2.27 N or O ligand atoms at approximately 1.75 Å, and 0.68 Mn atoms at approximately 2.69 Å. The uncertainties in distances are estimated at ±0.03 Å, while errors in the number of neighbors are estimated at ±20% or even higher. These data have been interpreted as a dinuclear Mn_2 unit (Mn···Mn = 2.69 Å) bridged by oxide ligands (Mn–O = 1.75 Å) and with peripheral O,N-based ligation (Mn–L = 1.98 Å). Recent refinements of the EXAFS data indicate the possible presence of additional Mn atoms separated by ~3.3 Å from the dinuclear pair, either as (i) two "mononuclear" sites or (ii) an additional Mn_2 unit (Mn···Mn = 2.69 Å) yielding a dimer-of-dimers, separated by approximately 3.3 Å. Synthetic molecules possessing these qualitative features have hitherto been unknown, but it can be readily seen that complex **4** does reproduce these features. The short "hinge-hinge" and long "hinge-wing-tip" separations correspond to the two separations from the EXAFS fit and with interpretation (i) above.

Overall, complex **4** possesses several features which are similar to those of the native S_1 site and which thus make it attractive as a potential model: (a) a metal nuclearity of four; (b) oxide bridges between the metal centers; (c) O,N-based peripheral ligation; (d) average metal oxidation state of +3.0; (e) two inequivalent types of Mn atoms ("hinge" and "wing-tip"); and (f) metric parameters consistent with the EXAFS fits. It can be seen in Table VII that metric parameters are, in some cases, slightly beyond the limits estimated for the EXAFS fit, but a better quantitative comparison must await parameters measured by identical techniques. Note also that the short Mn···Mn separation in **1** (2.779 (1) Å) now brings this parameter within the error uncertainly of the EXAFS fit and suggests similar variations at the Mn^{III}_4 oxidation level in the synthetic complexes may be possible. Overall, even though complex **4** may not reproduce exactly all the structural features of the native S_1 state, it nevertheless suggests that a close approach to the native site may be at hand.

With all the above comparisons suggesting that complex **4** provides a potential synthetic representation of the native S_1 site, correspondence can be extended to the other S_n states. Complex **2**, with its +2.75 average Mn oxidation level, would correspond to the S_0 state—the most reduced form of the water oxidation site participating in the catalytic cycle.[8] We have been thwarted in our attempts to structurally characterize this complex, but available evidence is consistent with it being isostructural with **4**. Similarly, complex **1** has an average metal oxidation state of +2.50 and would correspond to the "super-reduced" state, S_{-1}, which does not participate in the catalytic cycle but can be adopted by the native site of cyanobacteria in the dark[10] and can be artificially generated in spinach chloroplasts by treatment with H_2O_2.[9] The combined results, therefore, suggest that three oxidation levels of the water oxidation site may have been obtained, as summarized in the following scheme where equivalent oxidation levels are presented in the same column. The electrochemical

$$\underset{\substack{Mn^{2.50+}\\ \mathbf{1}}}{S_{-1}} \xrightarrow{-e^-} \underset{\substack{Mn^{2.75+}\\ \mathbf{2}}}{S_0} \xrightarrow{-e^-} \underset{\substack{Mn^{3.00+}\\ \mathbf{4}}}{S_1}$$

interconvertibility of **2** and **9** supports this. The S_{-1} model **1** can also be oxidized to the $Mn^{2.75+}$ level, and it could be speculated that the S_{-1} level in the native system is oxidized to S_0 with binding of an additional carboxylate to yield a species corresponding to **2**, ready for participation in the catalytic cycle. The potentials of the "S_{-1}/S_0" and "S_0/S_1" couples in the models are within the capability of the $PSII^+$ electron acceptor (~1 V vs NHE; ~0.6 V vs Fc). The potential required to generate the $[Mn_4O_2]^{9+}$ core is, however, rather positive (0.87 V vs Fc, ~1.3 V vs NHE) and, even allowing for variations of potential with medium, may well be beyond the capability of the $PSII^+$ acceptor. This indicates that an additional process might be necessary to reduce the potential of this "S_1/S_2" couple. Indeed, a number of recent investigations have shown that binding of small molecules such as water (substrate) or NH_3 occurs during the S_1-to-S_2 oxidation. Thus, in the same way that binding of a seventh carboxylate lowers the oxidation potential of the $Mn^{2.5+}_4 \rightarrow Mn^{2.75+}_4$ transition (by ~1 V) binding of H_2O (as OH^- or O^{2-}) lowers the potential of the S_1/S_2 couple to within the ability of $PSII^+$. Thus, we propose that the $[Mn_4O_2]$ species may represent models of the S_{-1}–S_1 states but that the higher S_n states are structurally different. Note that we have recently reported[49] the preparation of species containing the $[Mn_4O_3]^{7+}$ core ($3Mn^{III}$,Mn^{IV}) corresponding to S_2 and that they can be considered as the Mn_4O_2 core with an additional O^{2-} bridging the two "wing-tip" and one of the "hinge" Mn centers. We have incorporated these ideas into a mechanistic model of the

(46) (a) Dismukes, G. C.; Ferris, K.; Watnick, P. *Photochem. Photobiol.* **1982**, *3*, 243. (b) Hansson, O.; Aasa, R.; Vanngard, T. *Biophys. J.* **1987**, *51*, 825. (c) Siderer, Y.; Dismukes, G. C. *Proc. Natl. Acad. Sci. U.S.A.* **1981**, *78*, 274.

(47) (a) Dismukes, G. C.; Damoder, R. *Biophys. J.* **1985**, *47*, 166a. (b) Brudvig, G. W. *Metal Clusters in Proteins*; Que, L., Ed.; ACS Symposium Series 372; American Chemical Society: Washington, DC, 1988; Chapter 11.

(48) (a) Yachandra, V. K.; Guiles, R. D.; McDermott, A.; Britt, R. D.; Dexheimer, S. L.; Sauer, K.; Klein, M. P. *Biochim. Biophys. Acta* **1986**, *850*, 324. (b) Guiles, R. D.; Yachandra, V. K.; McDermott, A. E.; Britt, R. D.; Dexheimer, S. L.; Sauer, K.; Klein, M. P. *Proc. VII Int. Congr. Photosynthesis*, in press.

(49) Bashkin, J. S.; Chang, H.-R.; Streib, W. E.; Huffman, J. C.; Hendrickson, D. N.; Christou, G. *J. Am. Chem. Soc.* **1987**, *109*, 6502.

water oxidation cycle,[50a] a recently modified[50b,c] version of which incorporates the Mn_4O_3 core at S_2. We have also proposed that S_3 now possesses the second substrate (H_2O) molecule in a deprotonated form to yield a $[Mn_4O_4]^{6+}$ core at S_3; again, binding of a second hard ligand (as OH^- or O^{2-}) is proposed to lower the potential of the S_2/S_3 couple to within the $PSII^+$ limit. Thus, a synergistic relationship is proposed: the Mn_4O_2 core acts as a template to bind, deprotonate, bring together, and facilitate oxidative coupling of the two H_2O molecules to O_2, and, in return, the bound substrates lower the potential required to access the higher S_n states; this is summarized below. Subsequent oxidation

$$[Mn_4O_2]^{7+} \underset{S_0}{\xrightarrow{-e}} [Mn_4O_2]^{8+} \underset{S_1}{\xrightarrow[-2H^+]{-e,\ +H_2O}} [Mn_4O_3]^{7+} \underset{S_2}{\xrightarrow[-2H^+]{-e,\ +H_2O}} [Mn_4O_4]^{6+} \underset{S_3}{}$$

to S_4 spontaneously evolves O_2 returning the Mn assembly to $[Mn_4O_2]^{7+}$ (S_0). More detail will be provided with our full report of the $[Mn_4O_3]^{7+}$-containing products.

Summary and Conclusions

Treatment of trinuclear complexes containing the Mn_3O core with chelating bipy allows high-yield access into a new class of tetranuclear Mn complexes containing the Mn_4O_2 core. The products can be obtained in three different oxidation levels by appropriate choice of the Mn_3O reagent employed. The Mn_4O_2 complexes possess structural and other features bearing correspondence to the native site of the water oxidation system, suggesting that synthetic models of the latter in its S_{-1}, S_0, and S_1 states may have been obtained. A search for tetranuclear species corresponding to the S_2 and S_3 native levels is in progress, and preliminary work has been communicated.[49] Overall, availability of low molecular weight synthetic representations should prove invaluable in the continuing multidisciplinary investigation of the precise structure and mode of action of this important and complex biological system.

Acknowledgment. This work was supported by NSF Grant CHE-8507748 (to G.C.), by NIH Grant HL13652 (to D.N.H.), and we thank the Bloomington Academic Computing Service for a gift of computer time. C.C. thanks the Chemistry Department at Indiana University for Ira E. Lee and Harry G. Day Undergraduate Research Scholarships. NMR instrumentation at Indiana University was funded by NSF Grant CHE-8105004.

Supplementary Material Available: Complete listings of atomic coordinates, isotropic and anisotropic thermal parameters, bond lengths and angles, magnetic susceptibility and magnetization, and EPR data (24 pages); listings of observed and calculated structure factors for **1** and **4** (15 pages). Ordering information is given on any current masthead page. Complete copies of the MSC structure reports (No. 86162 and No. 86084 for **1** and **4**, respectively) are available on request from the Indiana University Chemistry Library.

(50) (a) Vincent, J. B.; Christou, G. *Inorg. Chim. Acta* **1987**, *L41*, 136. (b) Christou, G.; Vincent, J. B. *Metal Clusters in Proteins*; Que, L., Ed.; ACS Symposium Series 372; American Chemical Society: Washington, DC, 1988; Chapter 12. (c) Christou, G.; Vincent, J. B. *Biochim. Biophys. Acta* **1988**, *895*, 259.

(51) See Supplementary Material.

Insertions of Electrophiles into Metal–Carbon Bonds: Formation of New Carbon–Nitrogen Linkages Mediated by the (η^5-Cyclopentadienyl)dinitrosylchromium Group[1,2]

Peter Legzdins,*[,3a] George B. Richter-Addo,[3a] Berend Wassink,[3a,4] Frederick W. B. Einstein,[3b] Richard H. Jones,[3b] and Anthony C. Willis[3b,5]

Contribution from the Departments of Chemistry, The University of British Columbia, Vancouver, British Columbia, Canada V6T 1Y6, and Simon Fraser University, Burnaby, British Columbia, Canada V5A 1S6. *Received July 7, 1988*

Abstract: Electrophiles NE^+ (E = O, p-$O_2NC_6H_4N$, or S) undergo unprecedented insertions into the Cr–C σ bonds of $CpCr(NO)_2R$ complexes (Cp = η^5-C_5H_5; R = Me, CH_2SiMe_3, or Ph) to afford $[CpCr(NO)_2\{N(E)R\}]^+$ cationic complexes. Present evidence is consistent with these insertions occurring via charge-controlled, intermolecular attacks by NE^+ at the Cr–R groups in classical S_E2 processes. When R = Me and E = O, the initially formed product isomerizes intramolecularly to the novel formaldoxime complex, $[CpCr(NO)_2\{N(OH)CH_2\}]^+$, which is isolable as its PF_6^- salt. Single crystals of this salt and that resulting from the reaction of $[p\text{-}O_2NC_6H_4N_2]^+BF_4^-$ with $CpCr(NO)_2Me$ have been subjected to X-ray crystallographic analyses. $[CpCr(NO)_2\{N(OH)CH_2\}]^+PF_6^-$ crystallizes in the monoclinic space group $P2_1/c$ with cell dimensions a = 7.903 (3) Å, b = 12.192 (2) Å, c = 13.417 (5) Å, and β = 95.59 (3)°. Similarly, crystals of $[CpCr(NO)_2\{N(NC_6H_4NO_2)Me\}]^+BF_4^-$ are also monoclinic, space group $P2_1/c$, but with cell dimensions a = 8.300 (1) Å, b = 16.964 (2) Å, c = 12.536 (2) Å, and β = 101.87 (1)°. The structures of the complexes were refined to final R_F values of 0.045 and 0.054, respectively. The most chemically interesting feature of both molecular structures is that the newly formed formaldoxime and p-nitrophenylmethyldiazene ligands function as Lewis bases through nitrogen atoms toward the formally 16-electron $[CpCr(NO)_2]^+$ cations. These ligands may be displaced from the chromium's coordination sphere by the more strongly coordinating Cl^- anion. The resulting $CpCr(NO)_2Cl$ can be reconverted to $CpCr(NO)_2R$ by treatment with the appropriate Grignard or organoaluminum reagent, thereby completing a cycle by regenerating the initial organometallic reactant. The entire sequence of stoichiometric reactions forming the cycle thus constitutes a selective method for the formation of new carbon–nitrogen bonds, the net organic conversions mediated by the $CpCr(NO)_2$ group being $NE^+ + R^- \rightarrow N(E)R$.

Complexes containing σ-bonded organic ligands play a central role in transition-metal organometallic chemistry.[6] Of the various chemical properties exhibited by these complexes, probably none is more important than their ability to undergo insertion reactions

0002-7863/89/1511-2097$01.50/0